

# Phase diagram of the spin-1/2 Kitaev-Gamma chain and emergent SU(2) symmetry

Wang Yang,<sup>1</sup> Alberto Nocera,<sup>1</sup> Tarun Tummuru,<sup>1</sup> Hae-Young Kee,<sup>2</sup> and Ian Affleck<sup>1</sup>

<sup>1</sup>*Department of Physics and Astronomy and Stewart Blusson Quantum Matter Institute, University of British Columbia, Vancouver, B.C., Canada, V6T 1Z1*

<sup>2</sup>*Department of Physics, University of Toronto, Ontario M5S 1A7, Canada*

We study the phase diagram of a one-dimensional version of the Kitaev spin-1/2 model with an extra “ $\Gamma$ -term”, using analytical, density matrix renormalization group and exact diagonalization methods. Two intriguing phases are found. In the gapless phase, although the exact symmetry group of the system is discrete, the low energy theory is described by an emergent SU(2)<sub>1</sub> Wess-Zumino-Witten (WZW) model. On the other hand, the spin-spin correlation functions exhibit SU(2) breaking prefactors, even though the exponents and the logarithmic corrections are consistent with the SU(2)<sub>1</sub> predictions. A modified nonabelian bosonization formula is proposed to capture such exotic emergent “partial” SU(2) symmetry. In the ordered phase, there is numerical evidence for an  $O_h \rightarrow D_4$  spontaneous symmetry breaking.

PACS numbers:

A quantum spin liquid is a phase of matter in which the constituent spins are highly entangled with each other without exhibiting any long range order [1–6]. The Kitaev spin-1/2 model on the two-dimensional (2D) honeycomb lattice is an exactly solvable spin liquid model [7], which has received considerable theoretical and experimental interest in the past decade [8–24] due to its potential in realizing quantum computers [25]. On the other hand, additional spin interactions allowed by the lattice symmetries inevitably exist in real materials. The Heisenberg term was first considered as a supplement to the Kitaev model [9]. Later it had been proposed that another off-diagonal term, dubbed the “ $\Gamma$ -term”, naturally arises in Kitaev materials [26], which dominates over the Heisenberg term and may even be crucial to stabilize the ferromagnetic (FM) Kitaev phase [27].

In one dimension (1D), strong quantum fluctuations make 1D spin liquids even more ubiquitous [28–32]. In many circumstances, strongly interacting 1D systems are more amenable to both analytical and numerical treatments. Methods having been proven successful in 1D include conformal field theory (CFT) [31, 33–36], bosonization [37–39], Bethe ansatz [40–44], and the density matrix renormalization group (DMRG) method [45–47]. Due to this reason, 1D physics is not only interesting in its own respect, but also useful in providing hints on strongly correlated physics in higher dimensions when an exact or controllable approach is lacking.

In this work, by combining the analytical, exact diagonalization (ED) and DMRG methods, we study the phase diagram of a 1D version of the Kitaev model with an extra  $\Gamma$ -term, termed as the spin-1/2 “Kitaev-Gamma chain”. The phase diagram is divided into a gapless phase and an ordered phase as shown in Fig. 1 (a). In the gapless phase, we find that the low energy theory is described by an emergent SU(2)<sub>1</sub> Wess-Zumino-Witten (WZW) model, although the exact symmetry group  $G \cong O_h \times \mathbb{Z}$  is discrete where  $O_h$  is the full octahe-

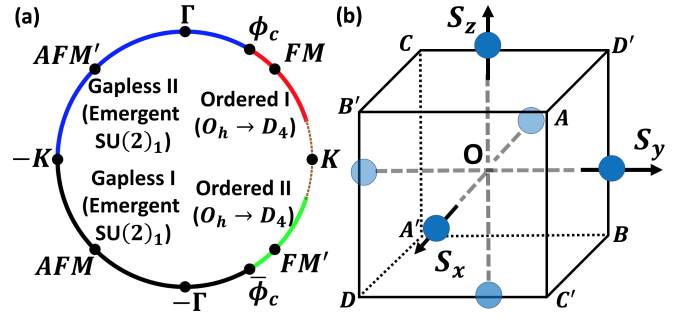


FIG. 1: (a) Phase diagram, and (b) a cube in spin space. In (a), the regions “Gapless I, II” are related by a three-sublattice rotation, and so are “Ordered I, II”. The region close to  $K$  represented by the thin dashed line remains to be explored further.

dral group. On the other hand, the spin-spin correlation functions exhibit SU(2) breaking prefactors as revealed by DMRG numerics, even though the exponents and the logarithmic corrections are consistent with SU(2)<sub>1</sub> predictions. A modified nonabelian bosonization formula for the spin operators is proposed to incorporate such emergent “partial” SU(2) symmetry. Based on a renormalization group (RG) analysis, the SU(2) breaking coefficients in the “bridge” between the local spin operators and the low energy degrees of freedom is attributed to a multiplicative renormalization of the spin operators in the high energy region along the RG flow before the SU(2)<sub>1</sub> low energy theory applies. In the ordered phase, ED and DMRG calculations show evidence of an  $O_h \rightarrow D_4$  spontaneous symmetry breaking where  $D_n$  represents the dihedral group of order  $2n$ , except in a small region close to the Kitaev point which remains to be explored further. We also discuss the relevance of our work to real materials and higher dimensional systems.

*The Model* The Hamiltonian of the spin-1/2 Kitaev-

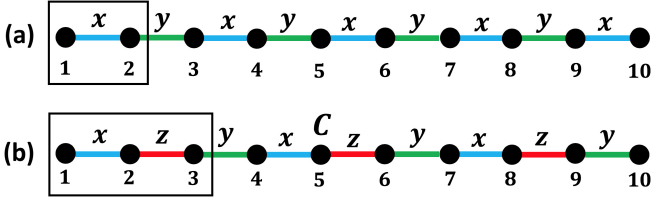


FIG. 2: Bond structures (a) before and (b) after the six-sublattice rotation. The rectangular boxes denote unit cells.

Gamma chain is defined as

$$H = \sum_{\langle ij \rangle \in \gamma \text{ bond}} [K S_i^\gamma S_j^\gamma + \Gamma (S_i^\alpha S_j^\beta + S_i^\beta S_j^\alpha)], \quad (1)$$

in which  $i$  and  $j$  are two nearest neighboring sites,  $\gamma = x$  (or  $y$ ) is the spin direction associated with the  $\gamma$ -bond,  $\alpha, \beta = y, z$  (or  $z, x$ ) on the  $\gamma$ -bond are the other two spin directions different from  $\gamma$ , and  $K = \cos(\phi)$  and  $\Gamma = \sin(\phi)$  are the Kitaev and Gamma couplings, respectively. The bond pattern shown in Fig. 2 (a) is generated by selecting out one row of the 2D Kitaev model on the honeycomb lattice [7]. Under a six-sublattice rotation [48, 49], the model can be mapped into the following form (see Supplementary Materials (SM) [50], which includes Refs. [1–4, 6, 55]),

$$H' = \sum_{\langle ij \rangle \in \gamma} [-K S_i^\gamma S_j^\gamma - \Gamma (S_i^\alpha S_j^\alpha + S_i^\beta S_j^\beta)], \quad (2)$$

in which the bonds  $\gamma = x, z, y$  depicted in Fig. 2 (b) have a three-site periodicity. Clearly,  $\phi = \pi/4$  and  $5\pi/4$  are SU(2) symmetric in the rotated frame with FM and antiferromagnetic (AFM) couplings, respectively.

From here on, we will stick to the rotated Hamiltonian in Eq. (2). The phase diagram is shown in Fig. 1 (a), in which  $\phi_c$  separating the gapless and ordered phases takes the value  $\approx 0.335\pi$  determined by numerics with evidence to be a first order phase transition (see SM [50]). Another three-sublattice rotation  $\mathcal{T}_3$  maps  $(K, \Gamma)$  to  $(K, -\Gamma)$  (see SM [50]), and as a result,  $\phi$  is equivalent to  $2\pi - \phi$ . There is numerical evidence for the exactly solvable [57] and self-dual  $K$  and  $-K$  points in Fig. 1 (a) to be a continuous and a first order phase transition point, respectively, as discussed in SM [50]. Due to the equivalence established by  $\mathcal{T}_3$ , we will focus on the range  $\phi \in [\pi, 2\pi]$  in the subsequent discussions. The Hamiltonian will be taken as  $H'$  and  $\mathcal{T}_3 H' \mathcal{T}_3^{-1}$  in the ranges  $[\pi, \bar{\phi}_c]$  and  $[\bar{\phi}_c, 2\pi]$ , respectively, where  $\bar{\phi}_c = 2\pi - \phi_c$ .

Next we discuss the symmetries of the model. The Hamiltonian in Eq. (2) has time reversal symmetry  $T$ . The bond structure is transformed back by applying either the screw operation  $R_a T_a$  or the combined operation  $R_I I$ , in which  $T_a$  is translation by one site,  $I$  is the spatial inversion around the site  $C$  shown in Fig. 2 (b),  $R_a : (S_i^x, S_i^y, S_i^z) \rightarrow (S_i^z, S_i^x, S_i^y)$  and

$R_I : (S_i^x, S_i^y, S_i^z) \rightarrow (-S_i^z, -S_i^y, -S_i^x)$  are rotations in spin space. The Hamiltonian is also invariant under spin rotations  $R(\hat{\alpha}, \pi)$  ( $\alpha = x, y, z$ ) where  $R(\hat{n}, \theta)$  represents a rotation around the  $\hat{n}$ -axis by an angle  $\theta$  in spin space. In summary, the symmetry group  $G$  is generated by the above mentioned operations, i.e.,  $G = \langle T, R_a T_a, R_I I, R(\hat{x}, \pi), R(\hat{y}, \pi), R(\hat{z}, \pi) \rangle$ .

The group structure of  $G$  can be worked out. A translation by three sites  $T_{3a} = (R_a T_a)^3$  generates an abelian normal subgroup  $\langle T_{3a} \rangle$  of  $G$ , hence it's legitimate to consider the quotient group  $G/\langle T_{3a} \rangle$ . The spin operations  $R_a, R_I, R(\hat{\alpha}, \pi)$  ( $\alpha = x, y, z$ ) are all symmetries of a cube in the spin space shown in Fig. 1 (b). Furthermore,  $T : \vec{S}_i \rightarrow -\vec{S}_i$  can be viewed as an improper element with determinant  $-1$  which also leaves the cube invariant. Indeed, these operations within the spin space generate the full octahedral group  $O_h$ . On the other hand, it's a pleasant result that  $G/\langle T_{3a} \rangle$  is isomorphic to  $O_h$  even if the spatial operations  $T_a$  and  $I$  are also included (see SM [50]). Thus  $G \cong O_h \times \mathbb{Z}$  where  $\mathbb{Z} \cong \langle T_{3a} \rangle$ .

*The gapless phase* We first briefly review the low energy theory at the SU(2) symmetric point  $\phi_{AF} = 5\pi/4$ . The low energy physics is described by the SU(2)<sub>1</sub> WZW model [31, 32, 58]. The nonabelian bosonization formula [31]  $\frac{1}{a} S_n^\alpha = J_L^\alpha(x) + J_R^\alpha(x) + \text{const.} (-)^{x/a} \frac{1}{\sqrt{a}} \text{itr}(g(x) \sigma^\alpha)$  relates the local spin operators to the low energy degrees of freedom in the SU(2)<sub>1</sub> WZW model, in which  $a$  is the lattice constant,  $x = na$  is the coordinate in the continuum limit,  $\vec{J}_L$  and  $\vec{J}_R$  are the left and right WZW currents, respectively,  $g$  is an SU(2) matrix which is also the WZW primary field, and  $\sigma^\alpha$  ( $\alpha = x, y, z$ ) are the three Pauli matrices. Since the scaling dimensions of  $g$  and the currents  $\vec{J}_L, \vec{J}_R$  are 1/2 and 1, respectively, the zero temperature equal-time spin-spin correlation functions in the long distance limit can be derived as  $\langle S_i^\alpha S_j^\beta \rangle = \delta_{\alpha\beta} [ -\frac{1}{4\pi^2} \frac{1}{r^2} + (-)^r \frac{1}{(2\pi)^{3/2}} \frac{\ln^{1/2}(r/r_0)}{r} ]$ , in which  $r = |i - j| \gg 1$ ,  $\langle \dots \rangle$  is an average over the ground state,  $r_0$  is some microscopic length scale, and the logarithmic correction arises from the marginally irrelevant term  $-\lambda \vec{J}_L \cdot \vec{J}_R$  [55, 59] where  $\lambda > 0$  is the coupling constant. For a periodic system of size  $L$ , the correlation functions can be obtained by replacing  $r$  with  $\frac{L}{\pi} \sin(\frac{\pi r}{L})$  [60].

Now we analyze the low energy field theory away from  $\phi_{AF}$ . In the vicinity of  $\phi_{AF}$ , the SU(2) breaking term  $(\Gamma - K) \sum_{\langle ij \rangle \in \gamma} S_i^\gamma S_j^\gamma$  can be treated as a perturbation to the SU(2)<sub>1</sub> WZW model. The dimension 1/2 operators  $\epsilon, N^\alpha$  and the dimension 3/2 operators  $J_L^\alpha \epsilon, J_R^\alpha \epsilon, J_L^\alpha N^\beta, J_R^\alpha N^\beta$  flip the sign under  $T_{3a}$  since  $T_a : g \rightarrow -g$  [31], where  $\epsilon(x) = \text{tr}g(x)$  and  $\vec{N}(x) = \text{itr}(g(x) \vec{\sigma})$  are the dimer and Neel order fields, respectively [31]. The dimension 1 operators  $J_L^\alpha, J_R^\alpha$  acquire a sign change under  $R(\hat{\beta}, \pi)$  ( $\beta \neq \alpha$ ). Hence they are all forbidden in the low energy theory. Among the dimension 2 operators, only the SU(2) invariant combinations  $\vec{J}_L \cdot \vec{J}_L + \vec{J}_R \cdot \vec{J}_R$  and  $\vec{J}_L \cdot \vec{J}_R$  are allowed by the  $O_h$  symmetry. Higher dimen-

sional operators are irrelevant at the CFT fixed point. Thus we conclude that there is an emergent  $SU(2)_1$  symmetry in a neighborhood of  $\phi_{AF}$ . Indeed, the finite size spectrum exhibits a conformal tower structure consistent with an emergent  $SU(2)_1$  symmetry (see SM [50]).

On the other hand, when  $\phi \neq \phi_{AF}$ , we propose the following modified nonabelian bosonization formula with  $SU(2)$  breaking coefficients:

$$\frac{1}{a} S_n^\alpha = [c_0 + c_4 \cos(\frac{2\pi}{3a}x + \frac{2\pi}{3}(\alpha - 1))] (J_L^\alpha(x) + J_R^\alpha(x)) + [c_6(-)^{\frac{x}{a}} + c_2 \cos(\frac{\pi}{3a}x + \frac{2\pi}{3}(\alpha - 1))] \frac{1}{\sqrt{a}} i \text{tr}(g(x)\sigma^\alpha), \quad (3)$$

in which  $\alpha = 1, 2, 3$  corresponding to  $\alpha = x, y, z$ , and  $x = na$ . As can be seen from Eq. (3),  $\langle S_1^\alpha S_{r+1}^\alpha \rangle$  now contains momentum  $\pm\pi/3$  and  $\pm 2\pi/3$  oscillating components in addition to the uniform part  $u_{\alpha\alpha}(r)$  and the staggered part  $(-)^r s_{\alpha\alpha}(r)$  where both  $u_{\alpha\alpha}$  and  $s_{\alpha\alpha}$  are smooth. Alternatively,

$$\langle S_i^\alpha S_j^\beta \rangle = \delta_{\alpha\beta} [-D_{[i]}^\alpha D_{[j]}^\alpha \frac{1}{r^2} + (-)^r C_{[i]}^\alpha C_{[j]}^\alpha \frac{\ln^{1/2}(r/r_0)}{r}], \quad (4)$$

in which  $1 \leq [i] \leq 3$ ,  $i \equiv [i] \pmod{3}$ ,  $r = |i - j|$ ,  $D_1^z = D_2^y = D_3^x = D_1 = c_0 + c_4$ ,  $D_1^x = D_1^y = D_2^z = D_2^y = D_3^x = D_3^z = D_2 = c_0 - c_4/2$ , and similar equalities hold for the  $C$ 's with  $C_1 = c_6 + c_2$  and  $C_2 = c_6 - c_2/2$ . Particularly, the relations between the  $D$ 's (also  $C$ 's) are dictated by symmetries (see SM [50]).

Next we proceed to numerics. Throughout the gapless phase, DMRG numerics are performed on a chain of  $L = 144$  sites with a periodic boundary condition. The DMRG results for the staggered parts  $s_{\alpha\alpha}(r)$  at  $\phi = 1.15\pi$  are displayed in Fig. 3 (a,b).  $s_{\alpha\alpha}$  ( $\alpha = x, y, z$ ) are extracted from the numerical data using a nine-point formula derived in SM [50]. In Fig. 3 (a), the slopes determined from a linear fit of  $\log s_{\alpha\alpha}(r)$  vs.  $\log(\sin(\pi r/L))$  are all close to  $-1$  within 5-10%, compatible with Eq. (4). To study the logarithmic corrections,  $(\sin(\pi r/L) s_{\alpha\alpha}(r))^2$  vs.  $\log(\sin(\pi r/L))$  are plotted in Fig. 3 (b) all exhibiting good linear relations, which confirm the logarithmic factor with a power of  $1/2$ .

We also study numerically in detail the  $SU(2)$  breaking factors in Eq. (4) at  $\phi = 1.15\pi$ . In Fig. 3 (e),  $(-)^r \sin(\pi r/L) \langle S_1^\alpha S_{r+1}^\alpha \rangle$  are observed to approach constant values at large  $r$  which are proportional to  $C_1^\alpha C_{[r+1]}^\alpha$  according to Eq. (4) [61]. To obtain  $D_1 D_2$ ,  $(D_1)^2$ ,  $(D_2)^2$ , we first pick out the data for every three sites, then  $u'_{i\alpha}(i + 3n - 1)$  defined as the uniform component of  $\{\sin(\pi(i + 3n - 1)/L) \langle S_1^\alpha S_{i+3n}^\alpha \rangle\}_{n \in \mathbb{Z}}$  as a function of  $n$  for fixed  $i$  and  $\alpha$  is extracted from a three-point formula [50], where  $\alpha = x, y, z$ , and  $i = 1, 2, 3$ . As is clear from Fig. 3 (c), a good linear fit for  $\log u'_{1x}(r)$  vs.  $\log(\sin(\pi r/L))$  is obtained with a slope close to  $-1$  within  $\sim 5\%$ . Hence the exponent of  $u'_{1x}(r)$  is determined to be around 2. Fig. 3 (d) displays the function  $d_{\alpha\alpha}(r)$  which is reconstructed from  $\sin(\pi r/L) u'_{i\alpha}(r)$  for a fixed  $\alpha$  but combining  $i =$

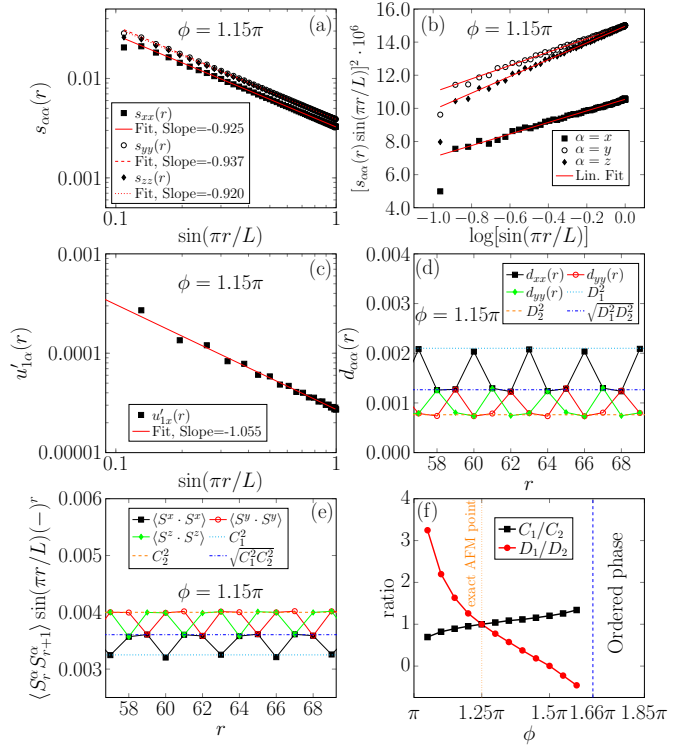


FIG. 3: (a)  $s_{\alpha\alpha}(r)$  vs.  $\tilde{r}_L (= \sin(\pi r/L))$  on a log-log scale, (b)  $(\tilde{r}_L s_{\alpha\alpha}(r))^2$  vs.  $\log \tilde{r}_L$ , (c)  $u'_{1x}(r)$  vs.  $\tilde{r}_L$  on a log-log scale, (d)  $d_{\alpha\alpha}(r)$  vs.  $r$ , (e)  $(-)^r \tilde{r}_L \langle S_1^\alpha S_{r+1}^\alpha \rangle$  vs.  $r$ , and (f)  $C_1/C_2$  and  $D_1/D_2$  as varying  $\phi$ , in which  $s_{\alpha\alpha}(r)$  is the staggered component of the correlation function  $\langle S_1^\alpha S_{r+1}^\alpha \rangle$ ;  $u'_{1x}(r)$  is the uniform component of  $\tilde{r}_L \langle S_1^x S_{r+1}^x \rangle$  where  $r$  is chosen every three sites;  $d_{\alpha\alpha}(r)$  ( $\alpha = x, y, z$ ) is reconstructed from  $\tilde{r}_L u'_{i\alpha}(r)$  by combining  $i = 1, 2, 3$  together;  $C_i, D_i$  ( $i = 1, 2$ ) are the  $SU(2)$  breaking coefficients in the modified nonabelian bosonization formula. In all of (a,b,c,d,e),  $\phi = 1.15\pi$ .

1, 2, 3 together, and  $D_1^\alpha D_i^\alpha$  can be determined from the asymptotic value of  $\sin(\pi r/L) u'_{i\alpha}(r)$  at large  $n$ , in which  $r = i + 3n - 1$ . We have verified that the independently extracted values of  $C_1 C_2 = a_1$ ,  $(C_1)^2 = a_2$ ,  $(C_2)^2 = a_3$  and  $D_1 D_2 = b_1$ ,  $(D_1)^2 = b_2$ ,  $(D_2)^2 = b_3$  indeed satisfy the relationships  $a_1 = \sqrt{a_2 a_3}$  and  $|b_1| = \sqrt{b_2 b_3}$ , which provide direct numerical evidence for Eq. (4). In addition, the ratios  $C_1/C_2$  and  $D_1/D_2$  are studied as a function of the angle  $\phi$  as shown in Fig. 3 (f), which provide evidence for emergent  $SU(2)_1$  in the entire AFM phase.

Finally, we present an RG argument to understand the origin of the  $SU(2)$  breaking coefficients. The following fermion Hamiltonian is considered

$$H_F = -t \sum_{\langle ij \rangle, \alpha} (c_{i\alpha}^\dagger c_{j\alpha} + \text{h.c.}) - \mu \sum_{i\alpha} c_{i\alpha}^\dagger c_{i\alpha} + U \sum_i n_{\uparrow} n_{i\downarrow} + \Delta \sum_{\langle ij \rangle \in \gamma} S_i^\gamma S_j^\gamma \quad (5)$$

in which  $t$  is the hopping term,  $\mu$  the chemical potential tuned to half-filling,  $U > 0$  is a repulsive Hubbard coupling,  $\Delta = \Gamma - K$ , and  $S_i^\gamma = c_{i\alpha}^\dagger \frac{1}{2} \sigma_{\alpha\beta}^\gamma c_{i\beta}$ . In the limit  $|\Delta| \ll U \ll t$ ,  $H_F$  contains the same low energy

physics in the spin sector as that of an SU(2) symmetric AFM Heisenberg chain perturbed by  $\Delta \sum_{\langle ij \rangle \in \gamma} S_i^\gamma S_j^\gamma$  [62]. To study the renormalization of spin operators, a term  $-\sum_{kn\alpha} h_k^\alpha(n) S_{k+3n}^\alpha$  can be added to  $H_F$ , in which  $k = 1, 2, 3$  are the site indices within a unit cell (u.c.),  $n$  is summed over the unit cells, and  $h_k^\alpha(n)$  are the scaling fields coupled to  $S_{i+3n}^\alpha$  which can be separated to a uniform part  $h_{u,k}^\alpha(n)$  and a staggered part  $(-)^{k+3n} h_{s,k}^\alpha(n)$ .

We study the flow of  $h_{\eta,k}^\alpha(n)$  ( $\eta = u, s, k = 1, 2, 3$ ) by lowering the cutoff from  $\Lambda_0 = \pi/a$  to  $\Lambda_1 \sim \Lambda_0/b_1$  close to the free fermion fixed point. The RG scale  $b_1$  can be taken as  $\sim 3$  where the three sites within a unit cell can no longer be clearly distinguished. Neglecting the flow of the marginal operator  $\Delta$  and keeping terms up to first order in  $\Delta$ , the flow equations of  $h_{\eta,k}^x(b, n)$  at scale  $\Lambda_0/b$  are

$$\begin{aligned} \frac{dh_{\eta,i}^x}{d \ln b} &= (1 - \nu_\eta \Delta) h_{\eta,i}^x - \lambda_\eta \Delta h_{\eta,j}^x - \nu_\eta \Delta h_{\eta,3}^x, \\ \frac{dh_{\eta,3}^x}{d \ln b} &= h_{\eta,3}^x, \end{aligned} \quad (6)$$

in which  $i, j = 1, 2, i \neq j$ ,  $\lambda_u = 0.14/t$ ,  $\nu_u = -0.07/t$ ,  $\lambda_s = -0.04/t$ ,  $\nu_s = 0.06/t$  (see SM [50]). In particular, the absence of  $\Delta$  in  $dh_{\eta,3}^x/d \ln b$  is due to the absence of  $S_{3+3n}^x$  in the  $\Delta$ -term of  $H_F$ . By solving Eq. (6), the coupling to the scaling fields at scale  $\Lambda_1$  can be obtained by coupling all the three  $h_{\eta,k}^x(b_1, n)$  to a same smeared spin operator  $S_{\eta,n}^x$ ,

$$\sum_{n \in \text{u.c.}} b_1 [A_\eta (h_{\eta,1}^x(n) + h_{\eta,2}^x(n)) + B_\eta h_{\eta,3}^x(n)] (-)^{\epsilon_\eta n} S_{\eta,n}^x, \quad (7)$$

in which  $\epsilon_\eta = 0, 1$  for  $\eta = u, s$ ,  $A_\eta = (1 - (\nu_\eta + \lambda_\eta) \Delta \ln b_1)$ ,  $B_\eta = (1 - 2\nu_\eta \Delta \ln b_1)$ , and  $h_{\eta,k}^x(n)$  are the bare fields at the scale  $\Lambda_0$ . Hence, a difference in the coefficients develops below the scale  $\Lambda_1$ . The ratio  $D_1/D_2$  ( $C_1/C_2$ ) is equal to  $B_\eta/A_\eta = 1 + (\lambda_\eta - \nu_\eta) \Delta$  with  $\eta = u$  ( $\eta = s$ ), which is linear in  $\phi$  for  $|\phi - \phi_{AF}| \ll 1$  of a negative (positive) slope, consistent with the numerical results shown in Fig. 3 (f). Similar analysis can be applied to the  $y$ - and  $z$ -directions.

*The ordered phase* We find numerical evidence of an  $O_h \rightarrow D_4$  spontaneous symmetry breaking for  $\bar{\phi}_c \leq \phi \lesssim 1.88\pi$ , except the  $FM'$  point at  $\phi = 7\pi/4$  where it is  $SU(2) \rightarrow U(1)$ . Since  $T_{3a}$  is unbroken, the spin orientations within a unit cell will be considered. The spin polarizations in one of the symmetry breaking ground states are

$$\langle \vec{S}_1 \rangle = S' \hat{z}, \langle \vec{S}_2 \rangle = S'' \hat{z}, \langle \vec{S}_3 \rangle = S'' \hat{z}, \quad (8)$$

in which  $\langle \vec{S}_i \rangle$  represents the expectation value of  $\vec{S}_i$  in the corresponding state,  $S'$  and  $S''$  are the magnitudes of the spin orders, and the little group of Eq. (118) is  $\langle R_a T_a R(\hat{z}, \pi) R_I IR(\hat{z}, \pi), T(R_a T_a)^{-1} R_I IR_a T_a \rangle \cong D_4$  modulo  $T_{3a}$  (see SM [50]). Hence, the symmetry breaking of Eq. (118) is  $O_h \rightarrow D_4$ , and the ‘‘center of mass’’

spin directions in the six (since  $|O_h/D_4| = 6$ ) distinct symmetry breaking ground states are along  $\pm \hat{x}, \pm \hat{y}, \pm \hat{z}$  shown as the six solid blue circles in Fig. 1 (b).

Next we discuss numerics. ED calculations show evidence of a six-fold ground state degeneracy at zero field, and one-fold, two-fold, three-fold degeneracies under small uniform fields  $h_z$  along  $\hat{z}$ ,  $h_{n_I}$  along  $\hat{n}_I$ , and  $h_{n_a}$  along  $\hat{n}_a$ , respectively. The fields  $h$ 's are chosen to satisfy  $\Delta E \ll hL \ll E_g$ , in which  $L$  is the system size,  $E_g$  is the excitation gap, and  $\Delta E$  is the finite size splitting of the ground state sextet at zero field. In addition, DMRG numerics show evidence of vanishing cross correlation functions  $\langle S_1^\alpha S_{r+1}^\beta \rangle$  ( $\alpha \neq \beta$ ) at any field, and nonzero diagonal correlations  $\langle S_1^\alpha S_{r+1}^\alpha \rangle$  for  $\alpha = z$  with  $h_z$ ,  $\alpha = x, z$  with  $h_{n_I}$  and  $\alpha = x, y, z$  with  $h_{n_a}$ . These results are all consistent with  $O_h \rightarrow D_4$ . However, ED show evidence of a four-fold ground state degeneracy at zero field when  $\phi \gtrsim 1.88\pi$  represented by the thin dashed line in Fig. 1 (a), which is incompatible with  $O_h \rightarrow D_4$ . Whether this is a finite size artifact or represents a different ordered phase remains to be explored.

Finally, we discuss the relevance of our study to real materials and higher dimensions. Since Kitaev and Gamma interactions are dominant in  $\alpha$ -RuCl<sub>3</sub>, 1D Kitaev-Gamma chain of Ruthenium stripes can be tailored using a- or b-axis oriented superlattices made of the Mott insulator RuCl<sub>3</sub>. Engineering of such 1D systems out of 2D layered materials has been successful in fabricating Iridium chain systems [63]. Furthermore, our results provide a starting point for an extrapolation to higher dimensions. The parameters relevant to real materials in 2D are FM for Kitaev and AFM for Gamma couplings [27, 64–66]. Thus the evolution of the 1D emergent  $SU(2)_1$  phase by increasing couplings between the chains is worth future studies which may offer further insights into possible spin liquid phases in  $\alpha$ -RuCl<sub>3</sub> systems.

In summary, we have studied the phase diagram of the spin-1/2 Kitaev-Gamma chain. In the gapless phase, the low energy physics is described by an emergent  $SU(2)_1$  WZW model, with  $SU(2)$  breaking coefficients in the modified nonabelian bosonization formula. In the ordered phase, DMRG and ED numerics provide evidence for an  $O_h \rightarrow D_4$  symmetry breaking except in a small region close to the Kitaev point.

We would like to thank A. Catuneanu for early contributions to this project. W. Y. and I. A. acknowledge support from NSERC Discovery Grant 04033-2016. H.-Y. K. acknowledges support from NSERC Discovery Grant 06089-2016, the Centre for Quantum Materials at the University of Toronto and the Canadian Institute for Advanced Research. A. N. acknowledges computational resources and services provided by Compute Canada and Advanced Research Computing at the University of British Columbia. A. N. is supported by the Canada First Research Excellence Fund.

- 
- [1] L. Balents, *Nature* **464**, 199 (2010).
- [2] W. Witczak-Krempa, G. Chen, Y. B. Kim, and L. Balents, *Annu. Rev. Condens. Matter Phys.* **5**, 57 (2014).
- [3] J. G. Rau, E. K.-H. Lee, and H.-Y. Kee, *Annu. Rev. Condens. Matter Phys.* **7**, 195 (2016).
- [4] S. M. Winter, A. A. Tsirlin, M. Daghofer, J. van den Brink, Y. Singh, P. Gegenwart, and R. Valenti, *J. Phys. Condens. Matter* **29**, 493002 (2017).
- [5] Y. Zhou, K. Kanoda, and T. K. Ng, *Rev. Mod. Phys.* **89**, 025003 (2017).
- [6] L. Savary, L. Balents, *Rep. Prog. Phys.* **80**, 016502 (2017).
- [7] A. Kitaev, *Ann. Phys. (N. Y.)* **321**, 2 (2006).
- [8] G. Jackeli and G. Khaliullin, *Phys. Rev. Lett.* **102**, 017205 (2009).
- [9] J. Chaloupka, G. Jackeli, and G. Khaliullin, *Phys. Rev. Lett.* **105**, 027204 (2010).
- [10] Y. Singh and P. Gegenwart, *Phys. Rev. B* **82**, 064412 (2010).
- [11] C. C. Price and N. B. Perkins, *Phys. Rev. Lett.* **109**, 187201 (2012).
- [12] Y. Singh, S. Manni, J. Reuther, T. Berlijn, R. Thomale, W. Ku, S. Trebst, and P. Gegenwart, *Phys. Rev. Lett.* **108**, 127203 (2012).
- [13] K. W. Plumb, J. P. Clancy, L. J. Sandilands, V. V. Shankar, Y. F. Hu, K. S. Burch, H. Y. Kee, and Y. J. Kim, *Phys. Rev. B* **90**, 041112 (2014).
- [14] H.-S. Kim, V. S. V., A. Catuneanu, and H.-Y. Kee, *Phys. Rev. B* **91**, 241110 (2015).
- [15] S. M. Winter, Y. Li, H. O. Jeschke, and R. Valenti, *Phys. Rev. B* **93**, 214431 (2016).
- [16] S. H. Baek, S. H. Do, K. Y. Choi, Y. Kwon, A. Wolter, S. Nishimoto, J. van den Brink, and B. Buchner, *Phys. Rev. Lett.* **119**, 037201 (2017).
- [17] I. A. Leahy, C. A. Pocs, P. E. Siegfried, D. Graf, S. H. Do, K. Y. Choi, B. Normand, and M. Lee, *Phys. Rev. Lett.* **118**, 187203 (2017).
- [18] J. A. Sears, Y. Zhao, Z. Xu, J. W. Lynn, and Y. J. Kim, *Phys. Rev. B* **95**, 180411 (2017).
- [19] A. U. B. Wolter, L. T. Corredor, L. Janssen, K. Nenkov, S. Schonecker, S. H. Do, K. Y. Choi, R. Albrecht, J. Hunger, T. Doert, M. Vojta, and B. Buchner, *Phys. Rev. B* **96**, 041405(R) (2017).
- [20] J. Zheng, K. Ran, T. Li, J. Wang, P. Wang, B. Liu, Z.-X. Liu, B. Normand, J. Wen, and W. Yu, *Phys. Rev. Lett.* **119**, 227208 (2017).
- [21] I. Rousochatzakis and N. B. Perkins, *Phys. Rev. Lett.* **118**, 147204 (2017).
- [22] Y. Kasahara, T. Ohnishi, N. Kurita, H. Tanaka, J. Nasu, Y. Motome, T. Shibauchi, and Y. Matsuda, *Nature (London)* **559**, 227 (2018).
- [23] A. Catuneanu, Y. Yamaji, G. Wachtel, Y. B. Kim, and H.-Y. Kee, *npj Quantum Mater.* **3**, 23 (2018).
- [24] M. Gohlke, G. Wachtel, Y. Yamaji, F. Pollmann, and Y. B. Kim, *Phys. Rev. B* **97**, 075126 (2018).
- [25] C. Nayak, S. H. Simon, A. Stern, M. Freedman, and S. Das Sarma, *Rev. Mod. Phys.* **80**, 1083 (2008).
- [26] J. G. Rau, E. K. H. Lee, and H. Y. Kee, *Phys. Rev. Lett.* **112**, 077204 (2014).
- [27] J. S. Gordon, A. Catuneanu, E. S. Sorenson, and H. Y. Kee, *Nat. Commun.* **10**, 2470 (2019).
- [28] F. D. M. Haldane, *Phys. Lett. A* **93**, 464 (1983).
- [29] F. D. M. Haldane, *Phys. Rev. Lett.* **50**, 1153 (1983).
- [30] I. Affleck, T. Kennedy, E. H. Lieb, and H. Tasaki, *Phys. Rev. Lett.* **59**, 799 (1987).
- [31] I. Affleck, in *Fields, Strings and Critical Phenomena*, Proceedings of Les Houches Summer School, 1988, edited by E. Brezin and J. Zinn-Justin (North-Holland, Amsterdam, 1990), pp. 563-640.
- [32] I. Affleck, *J. Phys. Condens. Matter* **1**, 3047 (1989).
- [33] A. Belavin, A. Polyakov, and A. Zamolodchikov, *Nucl. Phys. B* **241**, 333 (1984).
- [34] V. Knizhnik and A. Zamolodchikov, *Nucl. Phys. B* **247**, 83 (1984).
- [35] I. Affleck and F. D. M. Haldane, *Phys. Rev. B* **36**, 5291 (1987).
- [36] I. Affleck, *Acta Phys. Pol. B* **26**, 1869 (1995).
- [37] F. D. M. Haldane, *J. Phys. C* **14**, 2585 (1981).
- [38] F. D. M. Haldane, *Phys. Rev. Lett.* **47**, 1840 (1981).
- [39] E. Witten, *Commun. Math. Phys.* **92**, 455 (1984).
- [40] H. Bethe, *Zeitschrift f r Phys.* **71**, 205 (1931).
- [41] C. N. Yang and C. P. Yang, *Phys. Rev.* **150**, 327 (1966).
- [42] C. N. Yang and C. P. Yang, *Phys. Rev.* **150**, 321 (1966).
- [43] L. Faddeev, L. Takhtajan, and E. Sklyanin, *Theor. Math. Phys.* **40**, 688 (1979).
- [44] R. J. Baxter, *Exactly Solved Models in Statistical Mechanics* (Academic Press, London, 1982).
- [45] S. R. White, *Phys. Rev. Lett.* **69**, 2863 (1992).
- [46] S. R. White, *Phys. Rev. B* **48**, 10345 (1993).
- [47] U. Schollwock, *Ann. Phys. (N. Y.)* **326**, 96 (2011).
- [48] P. P. Stavropoulos, A. Catuneanu, and H. Y. Kee, *Phys. Rev. B* **98**, 104401 (2018).
- [49] J. Chaloupka, and G. Khaliullin, *Phys. Rev. B* **92**, 024413 (2015).
- [50] Supplementary Materials.
- [51] M. S. Dresselhaus, G. Dresselhaus, and A. Jorio, *Applications of Group Theory to the Physics of Solids* (Springer, New York, 2008) 1st ed.
- [52] P. Calabrese and J. Cardy, *J. Phys. A* **42**, 504005 (2009).
- [53] H. S. M. Coxeter, and W. O. Moser, *Generators and their relations for discrete groups* (Berlin: Springer 1965).
- [54] S. Eggert and I. Affleck, *Phys. Rev. B* **46**, 10866 (1992).
- [55] I. Affleck, D. Gepner, H. J. Schulz, and T. Ziman, *J. Phys. A. Math. Gen.* **22**, 511 (1989).
- [56] J. Cardy, *Scaling and Renormalization in Statistical Physics* (Cambridge University Press, Cambridge, 1996).
- [57] W. Brzezicki, J. Dziarmaga, and A. M. Oles, *Phys. Rev. B* **75**, 134415 (2007).
- [58] I. Affleck, *Phys. Rev. Lett.* **55**, 1355 (1985).
- [59] I. Affleck, *J. Phys. A. Math. Gen.* **31**, 4573 (1998).
- [60] V. Barzykin and I. Affleck, *J. Phys. A. Math. Gen.* **32**, 867 (1999).
- [61] The logarithmic correction in Eq. (4) is neglected in this treatment which does not affect the ratio  $C_1/C_2$  displayed in Fig. 3 (f).
- [62] Since a charge gap opens at infinitesimally small  $U$ , the low energy physics in the gapless spin sector of  $H_F$  when  $\Delta = 0$  is the same for both the weak and the large  $U$ , where the large  $U$  limit reproduces the AFM Heisenberg model.
- [63] J. H. Gruenewald, J. Kim, H. S. Kim, J. M. Johnson, J. Hwang, M. Souri, J. Terzic, S. H. Chang, A. Said, J. W. Brill, G. Cao, H.-Y. Kee, S. S. A. Seo, *Advanced Materials* **29**, 1603798 (2017).
- [64] H.-S. Kim and H.-Y. Kee, *Phys. Rev. B* **93**, 155143 (2016).

- [65] L. Janssen, E. C. Andrade, and M. Vojta, Phys. Rev. B **96**, 064430 (2017).
- [66] J. A. Sears, Li Ern Chern, Subin Kim, P. J. Bereciar-

tua, S. Francoual, Y. B. Kim, Y.-J. Kim, arXiv:1910.13390 (2019).

---

# Supplementary Materials

## Contents

<b>Acknowledgments</b>	4
<b>The sublattice rotations</b>	7
The six-sublattice rotation	7
The three-sublattice rotation and $(K, \Gamma) \cong (K, -\Gamma)$	8
Noncollinear FM-like quasi-long-range order in the unrotated frame	9
<b>Phase transitions</b>	11
Ground state energy as a function of $\phi$	11
Numerical determination of $\phi_c$	11
The central charge in the gapless region	12
<b>The symmetry operations</b>	12
Proof of $G / \langle T_{3a} \rangle \cong O_h$	12
Symmetry relations in the coefficients $C_{[i]}^\alpha$ 's and in $D_{[i]}^\alpha$ 's	16
<b>The nine- and three-point formulas</b>	18
The nine-point formula	18
The three-point formula	19
<b>SU(2)<sub>1</sub> conformal tower in the finite size spectrum</b>	19
<b>RG flows of the scaling fields</b>	21
Derivation of the RG flow equations	21
Solving the flow equations	27
<b>More on AFM phase</b>	28
DMRG numerics	28
Numerical study on the $\pi/3$ -oscillating components of the correlation functions	28
Finite size scaling of the exponents for the staggered parts of the correlation functions	29
Finite size scaling of $C_1/C_2$	29
<b>The FM phase</b>	30
Spin orientations with $O_h \rightarrow D_4$ symmetry breaking	30
ED results on the ground state degeneracies	32
DMRG results on the correlation functions in the FM phase	33
<b>References</b>	34

## THE SUBLATTICE ROTATIONS

### The six-sublattice rotation

Denoting  $H_{ij}$  to be the term in the Hamiltonian corresponding to the bond  $\langle ij \rangle$ , the unrotated Hamiltonian of the Kitaev-Gamma chain is

$$\begin{aligned}
 H_{12} &= K S_1^x S_2^x + \Gamma (S_1^y S_2^z + S_1^z S_2^y), \\
 H_{23} &= K S_2^y S_3^y + \Gamma (S_2^z S_3^x + S_2^x S_3^z), \\
 H_{34} &= H_{12}, (3 \rightarrow 1, 4 \rightarrow 2), \text{ etc.}
 \end{aligned} \tag{9}$$

The six-sublattice rotation is defined as

$$\begin{aligned}
\text{Sublattice 1: } & (x, y, z) \rightarrow (x', y', z'), \\
\text{Sublattice 2: } & (x, y, z) \rightarrow (-x', -z', -y'), \\
\text{Sublattice 3: } & (x, y, z) \rightarrow (y', z', x'), \\
\text{Sublattice 4: } & (x, y, z) \rightarrow (-y', -x', -z'), \\
\text{Sublattice 5: } & (x, y, z) \rightarrow (z', x', y'), \\
\text{Sublattice 6: } & (x, y, z) \rightarrow (-z', -y', -x'),
\end{aligned} \tag{10}$$

in which we have dropped the spin symbol  $S$  for simplicity. The Hamiltonian  $H'$  in the rotated basis becomes

$$\begin{aligned}
H'_{12} &= -K S_1^{x'} S_2^{x'} - \Gamma(S_1^{y'} S_2^{y'} + S_1^{z'} S_2^{z'}), \\
H'_{23} &= -K S_2^{z'} S_3^{z'} - \Gamma(S_2^{x'} S_3^{x'} + S_2^{y'} S_3^{y'}), \\
H'_{34} &= -K S_3^{y'} S_4^{y'} - \Gamma(S_3^{z'} S_4^{z'} + S_3^{x'} S_4^{x'}), \\
H'_{45} &= H'_{12}, (4 \rightarrow 1, 5 \rightarrow 2), \text{ etc.}
\end{aligned} \tag{11}$$

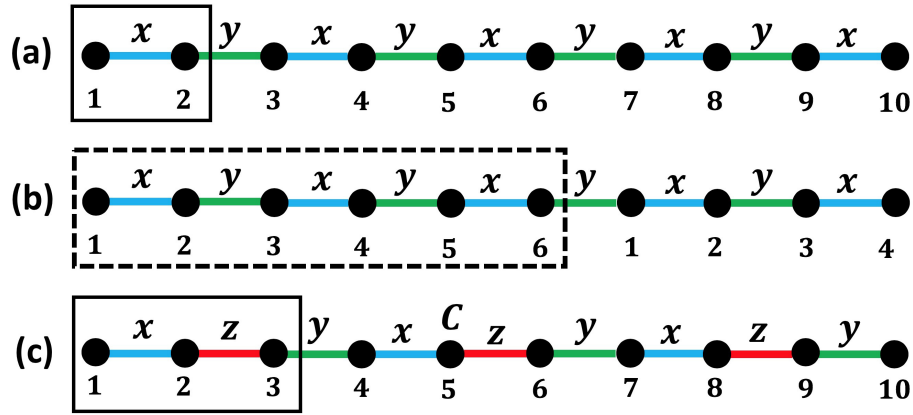


FIG. 4: (a,b) Bonds before and (c) after the six-sublattice rotation. In (a,c), the rectangular boxes represent unit cells of the lattice before and after six-sublattice rotation, respectively. In (b), the box represents a “unit” cell of the six-sublattice rotation, and the number at each site denotes the sublattice index in Eq. (10).

### The three-sublattice rotation and $(K, \Gamma) \cong (K, -\Gamma)$

In the unrotated frame, the three-sublattice rotation is defined as

$$\begin{aligned}
\text{Sublattice 1: } & (x, y, z) \rightarrow (x'', y'', z''), \\
\text{Sublattice 2: } & (x, y, z) \rightarrow (x'', -y'', -z''), \\
\text{Sublattice 3: } & (x, y, z) \rightarrow (x'', -y'', -z''),
\end{aligned} \tag{12}$$

and the Hamiltonian  $H$  is transformed into

$$\begin{aligned}
H''_{12} &= K S_1^{x''} S_2^{x''} - \Gamma(S_1^{y''} S_2^{y''} + S_1^{z''} S_2^{z''}), \\
H''_{23} &= K S_2^{y''} S_3^{y''} - \Gamma(S_2^{z''} S_3^{z''} + S_2^{x''} S_3^{x''}), \\
H''_{34} &= H''_{12}, (3 \rightarrow 1, 4 \rightarrow 2), \text{ etc.}
\end{aligned} \tag{13}$$

$D_4$	$E$	$C_2(z)$	$C_2(y)$	$C_2(x)$
$A$	1	1	1	1
$B_1$	1	1	-1	-1
$B_2$	1	-1	1	-1
$B_3$	1	-1	-1	1

TABLE I: Character table of  $D_2$  [1].

Alternatively, by performing the following three-sublattice rotation

$$\begin{aligned}
\text{Sublattice 1 : } (x, y, z) &\rightarrow (x''', y''', z'''), \\
\text{Sublattice 2 : } (x, y, z) &\rightarrow (x''', -y''', -z'''), \\
\text{Sublattice 3 : } (x, y, z) &\rightarrow (-x''', y''', -z'''),
\end{aligned} \tag{14}$$

to the rotated Hamiltonian  $H'$ , the transformed Hamiltonian  $H'''$  is

$$\begin{aligned}
H'''_{12} &= -K S_1'''^x S_2'''^x + \Gamma(S_1'''^y S_2'''^y + S_1'''^z S_2'''^z), \\
H'''_{23} &= -K S_2'''^z S_3'''^z + \Gamma(S_2'''^x S_3'''^x + S_2'''^y S_3'''^y), \\
H'''_{34} &= -K S_3'''^y S_4'''^y + \Gamma(S_3'''^z S_4'''^z + S_3'''^x S_4'''^x) \\
H'''_{45} &= H'''_{12}{}^K, (4 \rightarrow 1, 5 \rightarrow 2), \text{ etc.}
\end{aligned} \tag{15}$$

Indeed, in either case we verify that  $(K, \Gamma) \cong (K, -\Gamma)$ .

### Noncollinear FM-like quasi-long-range order in the unrotated frame

All physical properties of  $H$  in Eq. (9) can be obtained from those of  $H'$  in Eq. (11) by performing the inverse of the six-sublattice rotation in Eq. (10). In this section, we discuss the spin-spin correlation functions in the unrotated frame in the AFM phase based on the results within the rotated frame presented in the maintext. Throughout this section,  $S_i^\alpha$  and  $S_i'^\alpha$  represent a spin operator in the unrotated and rotated frames, respectively.

In the rotated frame, all the cross correlation functions vanish, i.e.,

$$\langle \Omega' | S_i'^\alpha S_j'^\beta | \Omega' \rangle = 0, \alpha \neq \beta, \tag{16}$$

in which  $|\Omega'\rangle$  is the ground state of  $H'$ . This is a consequence of the invariance of  $H'$  under  $R(\hat{\alpha}', \pi)$  ( $\alpha = x, y, z$ ) if the ground state does not break these symmetries (which is true in the AFM phase). For example, suppose  $R(\hat{x}', \pi)|\Omega'\rangle = |\Omega'\rangle$ . Then

$$\begin{aligned}
\langle \Omega' | S_i'^x S_j'^y | \Omega' \rangle &= \langle \Omega' | R^{-1}(\hat{x}', \pi) S_i'^x S_j'^y R(\hat{x}', \pi) | \Omega' \rangle \\
&= \langle \Omega' | R^{-1}(\hat{x}', \pi) S_i'^x R(\hat{x}', \pi) \cdot R^{-1}(\hat{x}', \pi) S_j'^y R(\hat{x}', \pi) | \Omega' \rangle \\
&= -\langle \Omega' | S_i'^x S_j'^y | \Omega' \rangle,
\end{aligned} \tag{17}$$

in which  $R^{-1}(\hat{x}', \pi) S_i'^x R(\hat{x}', \pi) = S_i'^x$  and  $R^{-1}(\hat{x}', \pi) S_j'^y R(\hat{x}', \pi) = -S_j'^y$  are used. From Eq. (17), it is clear that  $\langle \Omega' | S_i'^x S_j'^y | \Omega' \rangle = 0$ .

There is a group theoretical way to understand Eq. (16). Consider the group  $F$  generated by  $R(\hat{\alpha}', \pi)$  ( $\alpha = x, y, z$ ).  $F$  is isomorphic to  $D_2$  which is the dihedral group of order 4. To see this, note that the generator-relation representation of  $D_2$  is

$$D_2 = \langle a, b | a^2 = b^2 = (ab)^2 = e \rangle, \tag{18}$$

in which  $a, b$  are the two generators of  $D_2$ , and  $e$  is the identity element. In the group  $F$ , we identify  $a = R(\hat{x}', \pi)$  and  $b = R(\hat{y}', \pi)$ , and as a result, the product is  $ab = R(\hat{z}', \pi)$ . Hence, all the relations in Eq. (18) are satisfied, which shows that  $F$  is a subgroup of  $D_2$ . On the other hand, there are at least four elements in  $F$ , i.e., 1 and  $R(\hat{\alpha}', \pi)$  ( $\alpha = x, y, z$ ). Thus we conclude  $F \cong D_2$ . We also note that  $D_2$  has a direct product decomposition

$D_2 \cong \mathbb{Z}_2 \times \mathbb{Z}_2$ , and the corresponding decomposition of  $F$  is  $F = \{1, R(\hat{x}', \pi)\} \times \{1, R(\hat{y}', \pi)\}$ . With this preparation, we are able to interpret Eq. (18) in the language of group theory. The group  $D_2$  is abelian, hence only has one-dimensional irreducible representations. The character table of  $D_2$  [1] is shown in Table I, containing four irreducible representations  $A, B_1, B_2, B_3$ . Notice that  $S_i^z, S_i^y, S_i^x$  are in the  $B_1, B_2, B_3$  representations, respectively. Since the inner product between different irreducible representations vanishes [7], we conclude Eq. (16).

In the unrotated frame, Eq. (16) imposes constraints on the correlation functions by virtue of the six-sublattice rotation in Eq. (10). However, unlike Eq. (16), in the present case some of the cross correlations will be nonvanishing, while some of the diagonal correlations (*i.e.*,  $\langle S_i^\alpha S_i^\alpha \rangle$ ) are zero. Consider  $\langle \Omega | S_1^x S_{j+6n}^\alpha | \Omega \rangle$  as an example, in which  $|\Omega\rangle$  is the ground state of  $H$  in the unrotated frame,  $1 \leq j \leq 6$ , and  $n \in \mathbb{Z}$ . Denote  $U_6$  as the six-sublattice rotation, so that  $U_6 H U_6^{-1} = H'$ , and  $|\Omega'\rangle = U_6 |\Omega\rangle$ . Then

$$\begin{aligned} \langle \Omega | S_1^x S_{j+3n}^\alpha | \Omega \rangle &= \langle \Omega' | U_6 S_1^x S_{j+3n}^\alpha U_6^{-1} | \Omega' \rangle \\ &= \langle \Omega' | U_6 S_1^x U_6^{-1} \cdot U_6 S_{j+3n}^\alpha U_6^{-1} | \Omega' \rangle. \end{aligned} \quad (19)$$

Using Eqs. (10,16), we see that only the following correlations are nonzero,

$$\begin{aligned} \langle \Omega | S_1^x S_{1+3n}^x | \Omega \rangle &= \langle \Omega' | S_1^{t_x} S_{1+3n}^{t_x} | \Omega' \rangle, \\ \langle \Omega | S_1^x S_{2+3n}^x | \Omega \rangle &= -\langle \Omega' | S_1^{t_x} S_{2+3n}^{t_x} | \Omega' \rangle, \\ \langle \Omega | S_1^x S_{3+3n}^z | \Omega \rangle &= \langle \Omega' | S_1^{t_x} S_{3+3n}^{t_x} | \Omega' \rangle, \\ \langle \Omega | S_1^x S_{4+3n}^y | \Omega \rangle &= -\langle \Omega' | S_1^{t_x} S_{4+3n}^{t_x} | \Omega' \rangle, \\ \langle \Omega | S_1^x S_{5+3n}^y | \Omega \rangle &= \langle \Omega' | S_1^{t_x} S_{5+3n}^{t_x} | \Omega' \rangle, \\ \langle \Omega | S_1^x S_{6+3n}^z | \Omega \rangle &= -\langle \Omega' | S_1^{t_x} S_{6+3n}^{t_x} | \Omega' \rangle, \end{aligned} \quad (20)$$

and all other correlations vanish. In the long distance limit  $n \gg 1$ , all the six correlations in Eq. (20) are positive due to the staggered nature of the correlation functions in the rotated frame. Due to the  $\ln^{1/2}(r)/r$  power law decay behavior, Eq. (20) exhibits a noncollinear FM-like quasi-long-range order. Similar analysis can be performed on  $\langle \Omega | S_1^y S_{j+6n}^\alpha | \Omega \rangle$  and  $\langle \Omega | S_1^z S_{j+6n}^\alpha | \Omega \rangle$ .

Before closing this section, we further note that all the above analysis in the unrotated frame can alternatively be performed using the  $D_4$  group in the unrotated frame, which is given by  $\{1, U_6^{-1} R(\hat{x}', \pi) U_6, U_6^{-1} R(\hat{y}', \pi) U_6, U_6^{-1} R(\hat{z}', \pi) U_6\}$ . It is straightforward to work out the actions of  $U_6^{-1} R(\hat{\alpha}', \pi) U_6$ :

$$\begin{aligned} U_6^{-1} R(\hat{x}', \pi) U_6 : & \text{Sublattice 1. } R(\hat{x}, \pi) : (x, y, z) \rightarrow (x, -y, -z) \\ & \text{Sublattice 2. } R(\hat{x}, \pi) : (x, y, z) \rightarrow (x, -y, -z) \\ & \text{Sublattice 3. } R(\hat{z}, \pi) : (x, y, z) \rightarrow (-x, -y, z) \\ & \text{Sublattice 4. } R(\hat{y}, \pi) : (x, y, z) \rightarrow (-x, y, -z) \\ & \text{Sublattice 5. } R(\hat{y}, \pi) : (x, y, z) \rightarrow (-x, y, -z) \\ & \text{Sublattice 3. } R(\hat{z}, \pi) : (x, y, z) \rightarrow (-x, -y, z), \end{aligned} \quad (21)$$

$$\begin{aligned} U_6^{-1} R(\hat{y}', \pi) U_6 : & \text{Sublattice 1. } R(\hat{y}, \pi) : (x, y, z) \rightarrow (-x, y, -z) \\ & \text{Sublattice 2. } R(\hat{z}, \pi) : (x, y, z) \rightarrow (-x, -y, z) \\ & \text{Sublattice 3. } R(\hat{x}, \pi) : (x, y, z) \rightarrow (x, -y, -z) \\ & \text{Sublattice 4. } R(\hat{x}, \pi) : (x, y, z) \rightarrow (x, -y, -z) \\ & \text{Sublattice 5. } R(\hat{z}, \pi) : (x, y, z) \rightarrow (-x, -y, z) \\ & \text{Sublattice 3. } R(\hat{y}, \pi) : (x, y, z) \rightarrow (-x, y, -z), \end{aligned} \quad (22)$$

$$\begin{aligned} U_6^{-1} R(\hat{z}', \pi) U_6 : & \text{Sublattice 1. } R(\hat{z}, \pi) : (x, y, z) \rightarrow (-x, -y, z) \\ & \text{Sublattice 2. } R(\hat{y}, \pi) : (x, y, z) \rightarrow (-x, y, -z) \\ & \text{Sublattice 3. } R(\hat{y}, \pi) : (x, y, z) \rightarrow (-x, y, -z) \\ & \text{Sublattice 4. } R(\hat{z}, \pi) : (x, y, z) \rightarrow (-x, -y, z) \\ & \text{Sublattice 5. } R(\hat{x}, \pi) : (x, y, z) \rightarrow (x, -y, -z) \\ & \text{Sublattice 3. } R(\hat{x}, \pi) : (x, y, z) \rightarrow (x, -y, -z), \end{aligned} \quad (23)$$

in which ‘‘sublattice i’’ means all the lattice sites  $i + 6n$  where  $n \in \mathbb{Z}$ , and  $S_{i+3n}^\alpha$  is denoted as  $\alpha$  under ‘‘sublattice i’’ for short. Notice that the transformations acquire rather complicated forms in the unrotated frame. However, the group structure is still  $D_4$ , and equations like Eq. (20) are direct consequence of the symmetry operations in Eqs. (21,22,23).

## PHASE TRANSITIONS

### Ground state energy as a function of $\phi$

The ground-state energy  $E_0$  is a thermodynamic quantity that serves as an indicator of zero temperature phase transitions. The order of the transition is given by the first discontinuous derivative of  $E_0$ . In Fig. 5 (a), the ground state energy density  $E_0/L$  is shown as a function of  $\phi$  in the full parameter range calculated on a system of  $L = 36$  sites. Fig. 5 (b) plots the first order derivative  $\partial E_0/\partial\phi$  for three selective system sizes  $L = 12, 24, 36$ . There are clearly sudden jumps at  $\phi = \phi_c \sim 0.33\pi$  and  $\phi = \pi$ , indicating first order phase transitions. In addition, the size of the jump scales linearly with  $L$ , therefore, the discontinuity of the energy density  $E_0/L$  has a definite value in the thermodynamic limit. Fig. 5 (c) and (d) plot the second order derivative  $\partial^2 E_0/\partial\phi^2$  in the vicinities of  $\phi = \pi$  and  $\phi = \phi_c$ , respectively. The divergences at these two angles provide further confirmations for the occurrence of first order phase transitions.

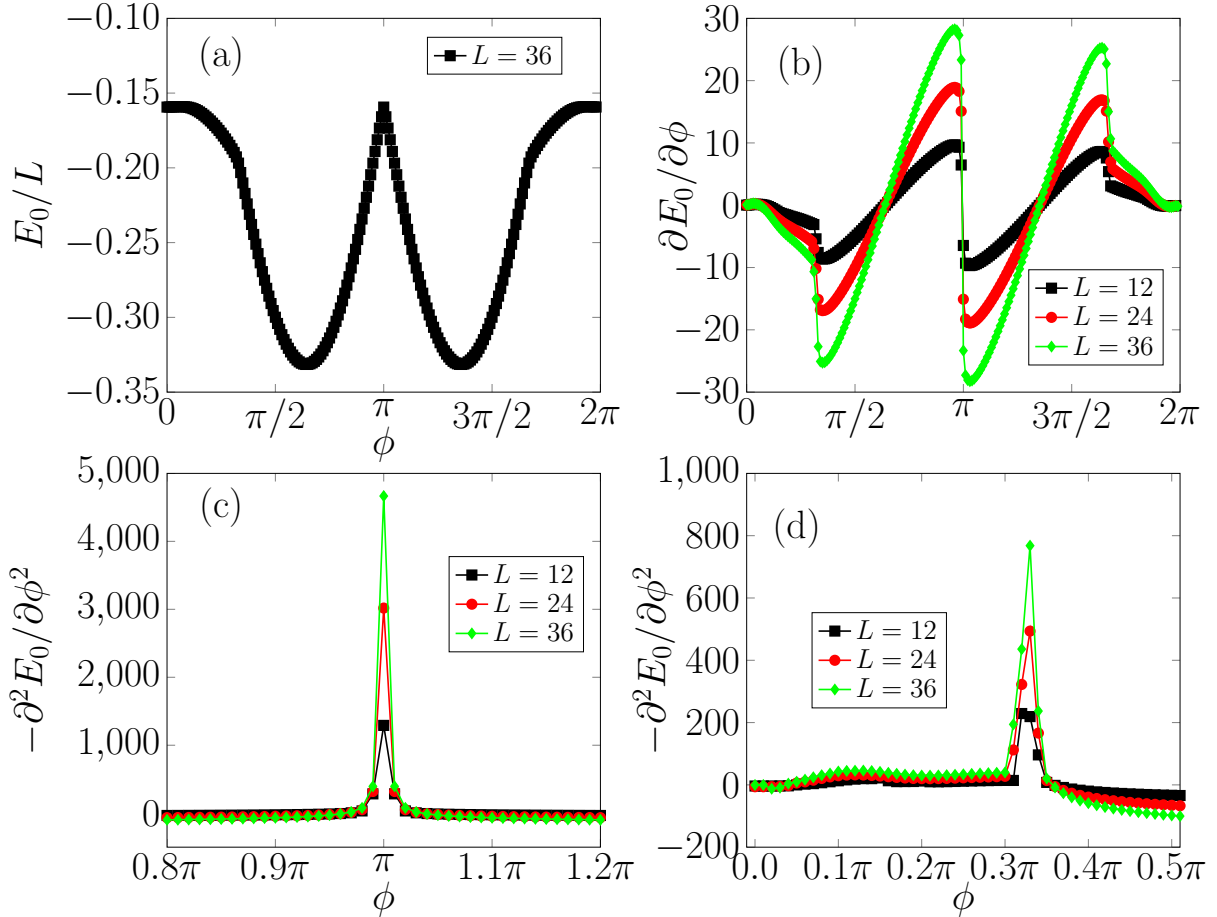


FIG. 5: (a)  $E_0/L$  and (b)  $\partial E_0/\partial\phi$  as functions of  $\phi$  in the full parameter range;  $\partial^2 E_0/\partial\phi^2$  in the vicinities of (c)  $\phi = \pi$  and (d)  $\phi = \phi_c$ . In (a), the system size is taken as  $L = 36$ . In (b,c,d), the plots include data for three different system sizes  $L = 12, 24, 36$ .

### Numerical determination of $\phi_c$

We determine  $\phi_c$  as the phase transition point separating the gapless and ordered phases with the following procedure. Fig. 6 (a) shows the gap  $\Delta = E_1 - E_0$  in the finite size spectrum for a system size of  $L = 28$  sites calculated using DMRG with open boundary conditions (OBC), where  $E_0$  is the energy of the ground state and  $E_1$  the energy of the first excited state. When chains with OBC are considered,  $m = 600$  DMRG states and up to 10 finite size

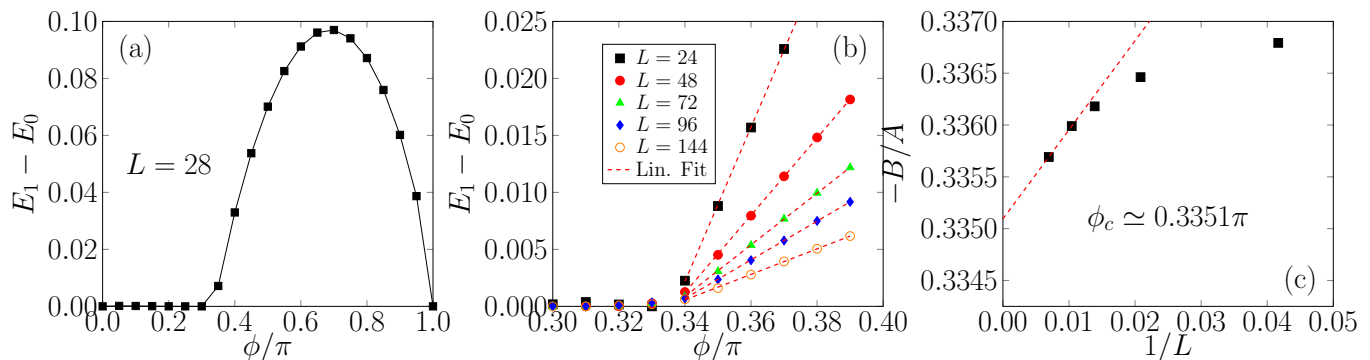


FIG. 6: (a)  $\Delta = E_1 - E_0$  as a function of  $\phi$  where  $E_0$  is the energy of the ground state and  $E_1$  the energy of the first excited state, (b)  $\Delta$  vs.  $\phi$  in the range  $\phi \in [0.3\pi, 0.4\pi]$  close to the phase transition point for several different system sizes  $L$ , and (c) the extrapolated value of  $\phi_c$  as a function of  $1/L$ . In (a),  $\Delta$  is calculated using DMRG on a system of  $L = 28$  sites with open boundary conditions ( $m = 600$  DMRG states were kept and up to 10 finite size sweeps were performed to reach convergence). In (b),  $\Delta$  is computed on a chain with periodic boundary conditions. In this case, to reach numerical convergence, up to  $m = 1000$  DMRG states were kept and tens of finite size sweeps were performed with a final truncation error of  $10^{-6}$ . In (c),  $\phi_c = -B/A$  is determined by extrapolating the fitted red linear dashed line in (b) to  $\Delta = 0$  at the corresponding  $L$ . The eventual value of  $\phi_c \approx 0.3351\pi$  in (c) is obtained by a linear extrapolation of the finite size  $\phi_c$  to  $L \rightarrow \infty$ .

sweeps were performed, with a final truncation error smaller than  $10^{-9}$ . The rounded dome structure appearing for  $\phi > 0.33\pi$  corresponds to the finite size gap in the gapless AFM phase. To determine the value of  $\phi_c$  more accurately, we zoomed in the interval  $0.3 < \phi < 0.4$  (Fig. 6 (b)). Here, several system sizes from  $L = 24$  up to  $L = 144$  are considered with periodic boundary conditions (PBC). The convergence of DMRG results was checked using up to  $m = 1000$  DMRG states and performing several tens of finite size sweeps, with a final truncation error smaller than  $10^{-6}$ . We emphasize that the use of chains with periodic boundaries is not necessary for the determination of the value of  $\phi_c$ . In fact, Fig. 6 (a) and Fig. 6 (b) provide evidence that the numerical results do not depend on the choice of boundary conditions.

In the gapless phase the finite size gap shows a perfect linear behavior as  $\Delta = A\phi + B$ . Fig. 6 (c) shows the extrapolated values of  $\phi_c = -B/A$  as a function of the inverse system size  $1/L$ . Finally the value  $\phi_c \simeq 0.3351\pi$  is obtained by extrapolating to the thermodynamic limit as shown by the red dashed line in Fig. 6 (c).

### The central charge in the gapless region

To extract the central charge of the critical phase, we study periodic systems of length  $L$  and compute the entanglement entropy  $S_L(x)$  of a subregion  $x$ . The entanglement, for a CFT with central charge  $c$ , is expected to scale as [2]

$$S_L(x) = \frac{c}{3} \ln \left[ \frac{L}{\pi} \sin \left( \frac{\pi x}{L} \right) \right] + \dots \quad (24)$$

A typical numerical fit for central charge, which we verified for multiple points in the gapless phase, is shown in Fig. 7. We find the  $c = 1$  to very good accuracy, thereby further corroborating the phase diagram.

## THE SYMMETRY OPERATIONS

### Proof of $G/ < T_{3a} > \cong O_h$

The full octahedral group  $O_h$  is the symmetry group of a cube as shown in Fig. 8, and is the largest among the five cubic point groups in three dimensional space.  $O_h$  contains 48 group elements. In  $O_h$ , there are 24 rotations which can be classified into five conjugacy classes  $\{E, 3C_2, 6C_4, 6C'_2, 8C_3\}$  where  $E$  represents the identity element. The actions of these 24 rotations on the x-, y- and z-axes and their geometrical meanings as symmetry operations of a cube are summarized in Table II. The other 24 elements of  $O_h$  are improper transformations with determinant  $-1$

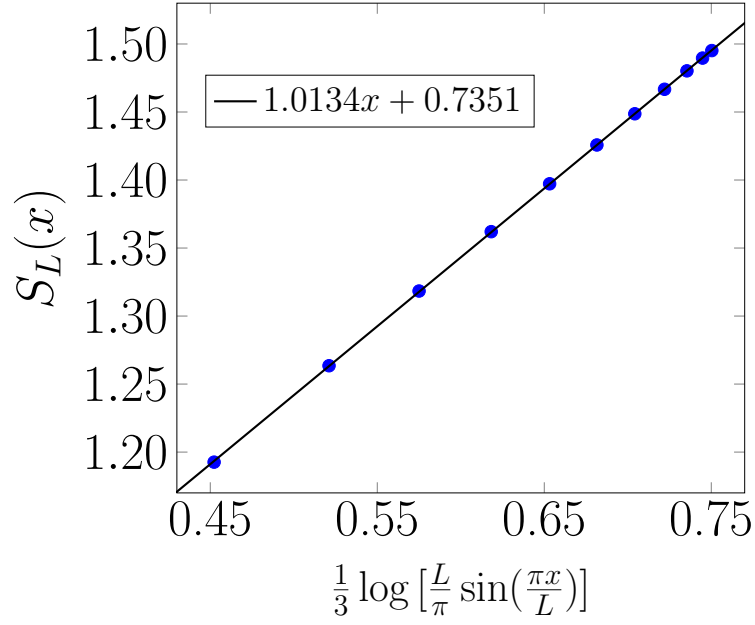


FIG. 7: Entanglement entropy  $S_L(x)$  of a subregion  $x$ , with rest of the system, in a periodic chain of length  $L = 30$ . This data has been obtained for the choice  $\phi = 0.85\pi$ . By fitting against the conformal distance on the horizontal axis, we obtain  $c = 1$ , which is consistent with the analytical analysis in the maintext.

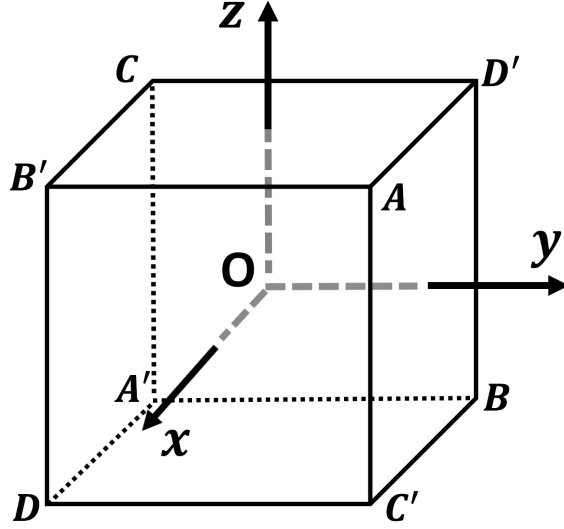


FIG. 8: A cube.

which can be obtained by multiplying the 24 rotations with the spatial inversion operation  $i$ . Correspondingly, the improper elements can also be classified into five conjugacy classes, *i.e.*,  $\{i, 3\sigma_h, 6S_4, 6\sigma_d, 8S_6\}$ .

There is a generator-relation representation for the  $O_h$  group [3]:

$$O_h = \langle r, s, t | r^2 = s^2 = t^2 = (rs)^3 = (st)^4 = (rt)^2 = e \rangle, \quad (25)$$

in which  $e$  is the identity element, and the geometrical meanings of the generators  $r, s, t$  as symmetry operations of a cube are three reflections. We are going to construct  $r, s, t$  out of  $T, R_a T_a, R_I I, R(\hat{x}, \pi), R(\hat{y}, \pi), R(\hat{z}, \pi)$ . Then we will show that on the one hand they indeed satisfy the above relations modulo  $T_{3a}$ , and on the other hand, the group generated by the constructed  $r, s, t$  contains at least 48 elements. Since  $|O_h| = 48$ , this proves that  $G/\langle T_{3a} \rangle$  is isomorphic to  $O_h$ .

Before proceeding on, we fix some notations. Let  $\mathcal{R}$  be a rotation in spin space defined as  $(\mathcal{R}(S^x), \mathcal{R}(S^y), \mathcal{R}(S^z)) =$

$E$	1	$(x, y, z)$	$\mathbb{1}$	$e$
$3C_2$	2	$(x, -y, -z)$	$R(OX, \pi)$	$r(ts)^2r$
	3	$(-x, y, -z)$	$R(OY, \pi)$	$sr(st)^2rs$
	4	$(-x, -y, z)$	$R(OZ, \pi)$	$(st)^2$
$6C_4$	5	$(x, z, -y)$	$R(OX, \frac{\pi}{2})$	$trsr$
	6	$(x, -z, y)$	$R(OX', \frac{\pi}{2})$	$rsrt$
	7	$(-z, y, x)$	$R(OY, \frac{\pi}{2})$	$rsts$
	8	$(z, y, -x)$	$R(OY', \frac{\pi}{2})$	$stsr$
	9	$(y, -x, z)$	$R(OZ, \frac{\pi}{2})$	$st$
	10	$(-y, x, z)$	$R(OZ', \frac{\pi}{2})$	$ts$
$6C_2'$	11	$(y, x, -z)$	$R([AC], \pi)$	$rsrtsr$
	12	$(-y, -x, -z)$	$R([BD], \pi)$	$r(ts)^2rst$
	13	$(z, -y, x)$	$R([AB], \pi)$	$rt$
	14	$(-z, -y, -x)$	$R([CD], \pi)$	$(st)^2rsts$
	15	$(-x, z, y)$	$R([AD], \pi)$	$strs$
	16	$(-x, -z, -y)$	$R([BC], \pi)$	$tsrtst$
$8C_3$	17	$(y, z, x)$	$R(OA, \frac{2\pi}{3})$	$rs$
	18	$(z, x, y)$	$R(OA', \frac{2\pi}{3})$	$sr$
	19	$(-y, -z, x)$	$R(OB, \frac{2\pi}{3})$	$trst$
	20	$(z, -x, -y)$	$R(OB', \frac{2\pi}{3})$	$tsrt$
	21	$(y, -z, -x)$	$R(OC, \frac{2\pi}{3})$	$stsrst$
	22	$(-z, x, -y)$	$R(OC', \frac{2\pi}{3})$	$tsrsts$
	23	$(-y, z, -x)$	$R(OD, \frac{2\pi}{3})$	$(st)^2rs$
	24	$(-z, -x, y)$	$R(OD', \frac{2\pi}{3})$	$sr(ts)^2$

TABLE II: List of 24 the group elements of the point group  $O$ . In accordance with the notations in Fig. 8,  $OM$  represents the vector pointing from the center of the cube (i.e. the point  $O$ ) to the vertex or the direction  $M$ , where  $M$  is one of  $A, A', B, B', C, C', D, D'$  when it is a vertex of the cube, and is one of  $X, Y, Z, X', Y', Z'$  when it represents a direction.  $X, Y, Z$  represent the positive directions of the three axes  $x, y, z$ , and  $X', Y', Z'$  represent the negative directions of the three axes. The symbol  $[MN]$  represents the line passing through the point that bisects the edge  $MN'$  and the point that bisects  $M'N$ , where  $M, N, M', N'$  are all vertices of the cube. The caption and the first four columns of the table are taken from W. Yang, T. Xiang, and C. Wu, Phys. Rev. B **96**, 144514 (2017).

$(S^x, S^y, S^z)R$ , in which  $R$  is a  $3 \times 3$  orthogonal matrix corresponding to  $\mathcal{R}$ . Let  $\mathcal{R}'$  be another rotation with  $R'$  the corresponding matrix. Then the composition  $\mathcal{R}\mathcal{R}'$  is given by

$$\mathcal{R}\mathcal{R}' : (S^x, S^y, S^z) \rightarrow (S^x, S^y, S^z)RR' \quad (26)$$

For later convenience, recall that  $R_a = R(\hat{n}_a, -2\pi/3)$  and  $R_I = R(\hat{n}_I, \pi)$  satisfy

$$\begin{aligned} R_a &: (S_i^x, S_i^y, S_i^z) \rightarrow (S_i^z, S_i^x, S_i^y), \\ R_I &: (S_i^x, S_i^y, S_i^z) \rightarrow (-S_i^z, -S_i^y, -S_i^x), \end{aligned} \quad (27)$$

in which  $\hat{n}_a = \frac{1}{\sqrt{3}}(1, 1, 1)^T$  is parallel to the line of  $OA$  in Fig. 8, and  $\hat{n}_I = \frac{1}{\sqrt{2}}(1, 0, -1)^T$  is parallel to the line passing through the point that bisects the edge  $CD'$  and the point that bisects  $C'D$  in Fig. 8. Hereafter within this section, the site index  $i$  will be dropped in subsequent discussions for simplifications of notations.

The constructions of  $r, s, t$  are as follows,

Generator	Expression	Spin space	Geometrical
$r$	$T \cdot R_I I$	$(x, y, z) \rightarrow (z, y, x)$	Reflection to $ABA'B'$ -plane
$s$	$T \cdot (R_a T_a)^{-1} \cdot R_I I \cdot R_a T_a$	$(x, y, z) \rightarrow (y, x, z)$	Reflection to $ACA'C'$ -plane
$t$	$T \cdot R(\hat{y}, \pi)$	$(x, y, z) \rightarrow (x, -y, z)$	Reflection to $xz$ -plane

(28)

in which the second, the third and the fourth columns give the expressions of  $r, s, t$  in terms of the symmetry operations  $T, R_a T_a, R_I I, R(\hat{x}, \pi), R(\hat{y}, \pi), R(\hat{z}, \pi)$  of the model, the actions in the spin space where  $S^\alpha$  is denoted as  $\alpha$  for short, and the geometrical meanings as symmetries of a cube in Fig. 8, respectively. Now we verify the relations  $r^2 = s^2 = t^2 = e$ . Firstly,

$$r^2 = T^2 \cdot I^2 \cdot (R_I)^2 = 1, \quad (29)$$

since  $T^2 = 1, I^2 = 1$  and  $(R_I)^2 = [R(\hat{n}_I, \pi)]^2 = R(\hat{n}_I, 2\pi) = 1$ . Secondly,

$$\begin{aligned} s^2 &= T^2 \cdot (T_a^{-1} I T_a)^2 \cdot (R_a^{-1} R_I R_a)^2 \\ &= T_{-a} I T_a \cdot T_{-a} I T_a \cdot [R(R_a^{-1} \hat{n}_I, \pi)]^2 \\ &= T_{-a} I^2 T_a \cdot R(R_a^{-1} \hat{n}_I, 2\pi) \\ &= 1, \end{aligned} \tag{30}$$

in which  $T_a^{-1} = T_{-a}$ , and  $R_0 R(\hat{n}, \theta) R_0^{-1} = R(R_0 \hat{n}, \theta)$  is used. Finally for  $t$ , we obtain

$$t^2 = T^2 \cdot [R(\hat{y}, \pi)]^2 = 1. \tag{31}$$

Using the expressions of  $r, s, t$ , it is straightforward to work out the expressions of  $rs, st, rt$ , as

Operation	Expression	Spin space	Geometrical	
$rs$	$(R_a T_a)^{-1}$	$(x, y, z) \rightarrow (y, z, x)$	$R(OA, \frac{2\pi}{3})$	(32)
$st$	$R_a T_a \cdot R(\hat{z}, \pi) \cdot R_I I \cdot R(\hat{z}, \pi)$	$(x, y, z) \rightarrow (y, -x, z)$	$R(\hat{z}, \frac{\pi}{2})$	
$rt$	$R(\hat{z}, \pi) \cdot R_I I \cdot R(\hat{z}, \pi)$	$(x, y, z) \rightarrow (z, -y, x)$	$R([AB], \pi)$	

in which  $[AB]$  represents the line passing through the point that bisects the edge  $AB'$  and the point that bisects  $A'B$  in Fig. 8. Next we verify the relations  $(rs)^3 = (st)^4 = (rt)^2 = e$ . Firstly,

$$\begin{aligned} (rs)^3 &= (R_a)^{-3} \cdot (T_a)^{-3} \\ &= [R(\hat{n}_a, -2\pi/3)]^{-3} \cdot T_{-3a} \\ &= R(\hat{n}_a, 2\pi) \cdot T_{-3a} \\ &= T_{-3a}, \end{aligned} \tag{33}$$

in which  $R_a = R(\hat{n}_a, -2\pi/3)$  is used, and clearly  $(rs)^3 = e$  modulo  $T_{3a}$ . Secondly,

$$\begin{aligned} (st)^4 &= (T_a I)^4 \cdot [R_a R(\hat{z}, \pi) R_I R(\hat{z}, \pi)]^4 \\ &= T_a (I T_a I) T_a (I T_a I) \cdot [R(\hat{z}, \pi/2)]^4 \\ &= T_a T_{-a} T_a T_{-a} \cdot R(\hat{z}, 2\pi) \\ &= 1, \end{aligned} \tag{34}$$

in which  $I T_a I = T_{-a}$  and  $R_a R(\hat{z}, \pi) R_I R(\hat{z}, \pi) = R(\hat{z}, \pi/2)$  are used. Finally,

$$\begin{aligned} (rt)^2 &= I^2 \cdot [R(\hat{z}, \pi) R_I R(\hat{z}, \pi)]^2 \\ &= [R(R(\hat{z}, \pi) \hat{n}_I, \pi)]^2 \\ &= 1. \end{aligned} \tag{35}$$

This proves that all the relations in Eq. (25) are satisfied. Hence  $G/\langle T_{3a} \rangle$  is isomorphic to a subgroup of  $O_h$ .

We note that the time reversal operation acquires a rather complicated form in terms of the generators. In fact, we have

Operation	Expression	Spin space	Geometrical	
$sr(st)^2r(st)$	$T$	$(x, y, z) \rightarrow (-x, -y, -z)$	Inversion of the cube	(36)

To verify the expression of  $T$ , using Eq. (28,32), one obtains

$$\begin{aligned} T &= (rs)^{-1} (st)^2 r(st) \\ &= (T_{-a})^{-1} (T_a I)^2 I (T_a I) \cdot R_a [R(\hat{z}, \pi/2)]^2 (T R_I) R(\hat{z}, \pi/2) \\ &= (T_a T_a) I (T_a (I I) T_a) I \cdot R_a R(\hat{z}, \pi) R_I R(\hat{z}, \pi/2) \cdot T. \end{aligned} \tag{37}$$

The spatial part of Eq. (37) is  $T_{2a} I T_{2a} I = T_{2a} T_{-2a} = 1$ . Using Eq. (27),  $R(\hat{z}, \pi) : (x, y, z) \rightarrow (-x, -y, z)$ ,  $R(\hat{z}, \pi/2) : (x, y, z) \rightarrow (y, -x, z)$ , and the composition rule Eq. (26), it is a straightforward calculation to verify that  $R_a R(\hat{z}, \pi) R_I R(\hat{z}, \pi/2) : (x, y, z) \rightarrow (x, y, z)$ . Thus  $sr(st)^2r(st)$  is equal to  $T$ .

Next we show that the quotient group  $G/\langle T_{3a} \rangle$  contains at least 48 elements. One can verify that by restricting the actions to the spin space, the 24 operations in the last column of Table II are exactly given by the third column of

Table II where  $\alpha$  is  $S^\alpha$  for short ( $\alpha = x, y, z$ ). This exhausts the 24 proper elements of the  $O_h$  group as a symmetry group of a cube in the spin space. Furthermore, by multiplying the 24 operations in the last column of Table II with  $T = (rs)^{-1}(st)^2r(st)$ , and again restricting to the spin space, we obtain the other 24 improper elements of the  $O_h$  group acting in the spin space. Then let's recover the spatial components of these 48 operations generated by  $r, s, t$ , and view them as elements in  $G/\langle T_{3a} \rangle$ . Since these 48 operations already act differently in the spin space from each other, they must be distinct elements in  $G/\langle T_{3a} \rangle$ . This shows that  $G/\langle T_{3a} \rangle$  has at least 48 group elements. Combining with the previously established fact that  $G/\langle T_{3a} \rangle$  is isomorphic to a subgroup of  $O_h$ , we conclude that  $G/\langle T_{3a} \rangle$  is actually isomorphic to  $O_h$ . We also note that the Hilbert space of the spin-1/2 Kitaev-Gamma chain is a projective representation of  $O_h$ , since a rotation by  $2\pi$  is  $-1$  for half-odd-integer spins.

We make a further comment on the group structure. Note that  $O_h = O \times \{1, i\}$  where “i” is the inversion. The cubic point group  $O$  has 24 elements and is isomorphic to  $S_4$ , the permutation group of four elements.  $S_4$  has a generator-relation representation as follows [3],

$$S_4 = \langle a, b, c | a^2 = b^3 = c^4 = abc = e \rangle, \quad (38)$$

or alternatively, it can also be generated by two generators,

$$O = \langle R, S | R^3 = S^4 = (RS)^2 = E \rangle. \quad (39)$$

We note that in our case, we can take

$$a = rt, b = rs, c = st, \quad (40)$$

and

$$R = rs, S = st. \quad (41)$$

### Symmetry relations in the coefficients $C_{[i]}^\alpha$ 's and in $D_{[i]}^\alpha$ 's

Suppose the spin operators  $S_i^\alpha$  at low energies can be written in terms of  $J_L^\alpha, J_R^\alpha, g$  as,

$$\frac{1}{a} S_i^\alpha = D_{[i]}^\alpha J_L^\alpha + D'_{[i]}^\alpha J_R^\alpha + C_{[i]}^\alpha \frac{1}{\sqrt{a}} (-)^{x/a} N^\alpha, \quad (42)$$

in which  $N^\alpha = i\text{tr}(g\sigma^\alpha)$ . We'll analyze what constraints the  $O_h$  symmetry will put on the coefficients.

First, consider the time reversal symmetry  $T$ . The transformations of  $S_i^\alpha, J_L^\alpha, J_R^\alpha$  and  $N^\alpha$  under  $T$  are

$$\begin{aligned} T : \quad S_i^\alpha &\rightarrow -S_i^\alpha \\ J_L^\alpha(x) &\rightarrow -J_R^\alpha(x) \\ J_R^\alpha(x) &\rightarrow -J_L^\alpha(x) \\ N^\alpha(x) &\rightarrow -N^\alpha(x). \end{aligned} \quad (43)$$

Performing time reversal transformation on both sides of Eq. (42), we obtain,

$$-\frac{1}{a} S_i^\alpha = -D_{[i]}^\alpha J_R^\alpha - D'_{[i]}^\alpha J_L^\alpha - C_{[i]}^\alpha \frac{1}{\sqrt{a}} (-)^{x/a} N^\alpha. \quad (44)$$

On the other hand, from Eq. (42),

$$-\frac{1}{a} S_i^\alpha = -D_{[i]}^\alpha J_L^\alpha - D'_{[i]}^\alpha J_R^\alpha - C_{[i]}^\alpha \frac{1}{\sqrt{a}} (-)^{x/a} N^\alpha. \quad (45)$$

Comparing Eq. (44) and Eq. (45), it is clear that

$$D_{[i]}^\alpha = D'_{[i]}^\alpha. \quad (46)$$

Next consider the symmetry operation  $R_a T_a$ . The transformations of  $S_i^\alpha$ ,  $J_L^\alpha$ ,  $J_R^\alpha$  and  $N^\alpha = \text{trg}(\sigma^\alpha)$  under  $R_a T_a$  are

$$\begin{aligned} R_a T_a : \quad S_i^\alpha &\rightarrow (R_a)^\alpha_\beta S_{i+1}^\beta \\ J_L^\alpha(x) &\rightarrow (R_a)^\alpha_\beta J_L^\beta(x) \\ J_R^\alpha(x) &\rightarrow (R_a)^\alpha_\beta J_R^\beta(x) \\ N^\alpha(x) &\rightarrow -(R_a)^\alpha_\beta N^\beta(x), \end{aligned} \quad (47)$$

in which  $(R_a)^\alpha_\beta$  is the matrix element of the vector representation of the rotation  $R_a$ , and the minus sign in the transformation of  $N^\alpha(x)$  is because  $T_a : g \rightarrow -g$ . Applying  $R_a T_a$  to  $S_1^x$ , under the same logic as the time reversal case, we obtain

$$D_2^z(J_L^z + J_R^z) + C_2^z \frac{1}{\sqrt{a}} (-)^{x/a+1} N^z = D_1^x(J_L^z + J_R^z) + C_1^x \frac{1}{\sqrt{a}} (-)^{x/a} (-) N^z, \quad (48)$$

from which

$$D_1^x = D_2^z, \quad C_1^x = C_2^z. \quad (49)$$

Similar analysis on other spin operators gives

$$\begin{aligned} C_1^x = C_2^z = C_3^y, \quad D_1^x = D_2^z = D_3^y \\ C_1^y = C_2^x = C_3^z, \quad D_1^y = D_2^x = D_3^z \\ C_1^z = C_2^y = C_3^x, \quad D_1^z = D_2^y = D_3^x. \end{aligned} \quad (50)$$

There is another symmetry  $R_I I$  in the  $O_h$  group. The transformations of  $S_i^\alpha$ ,  $J_L^\alpha$ ,  $J_R^\alpha$  and  $N^\alpha = \text{trg}(\sigma^\alpha)$  under  $R_I I$  are

$$\begin{aligned} R_I I : \quad S_i^\alpha &\rightarrow (R_I)^\alpha_\beta S_{-i}^\beta \\ J_L^\alpha(x) &\rightarrow (R_I)^\alpha_\beta J_R^\beta(-x) \\ J_R^\alpha(x) &\rightarrow (R_I)^\alpha_\beta J_L^\beta(-x) \\ N^\alpha(x) &\rightarrow (R_I)^\alpha_\beta N^\beta(-x). \end{aligned} \quad (51)$$

Applying  $R_I I$  to  $S_1^x$ , we obtain

$$-D_3^z(J_L^z(-x) + J_R^z(-x)) - C_3^z \frac{1}{\sqrt{a}} (-)^{-x/a} N^z(-x) = -D_1^x(J_L^z(-x) + J_R^z(-x)) - C_1^x \frac{1}{\sqrt{a}} (-)^{x/a} N^z(-x), \quad (52)$$

which gives

$$D_1^x = D_3^z, \quad C_1^x = C_3^z. \quad (53)$$

In summary, by using the  $O_h$  symmetry, we are able to show the following relations

$$\begin{aligned} D_1^z = D_2^y = D_3^x (= D_1), \\ D_1^x = D_2^z = D_3^y = D_1^y = D_2^x = D_3^z (= D_2), \end{aligned} \quad (54)$$

and

$$\begin{aligned} C_1^z = C_2^y = C_3^x (= C_1), \\ C_1^x = C_2^z = C_3^y = C_1^y = C_2^x = C_3^z (= C_2). \end{aligned} \quad (55)$$

Note that the difference in  $D_1$ ,  $D_2$  and in  $C_1$ ,  $C_2$  will introduce a  $4k_f$  and a  $2k_f$  oscillating component in the nonabelian bosonization formula, respectively, where  $k_f = \pi/6a$ . We now separate the components with different

momenta in  $D_{[i]}^x$  by performing a Fourier transformation. Other directions and the  $C_{[j]}^\alpha$ 's can be treated in a similar manner. Let

$$D_{[j]}^x = A \cos\left(\frac{2\pi}{3}j + \psi\right) + B. \quad (56)$$

Then

$$\begin{aligned} A \cos\left(\frac{2\pi}{3} + \psi\right) + B &= D_2 \\ A \cos\left(\frac{4\pi}{3} + \psi\right) + B &= D_2 \\ A \cos(\psi) + B &= D_1, \end{aligned} \quad (57)$$

which solves

$$\begin{aligned} A &= \frac{2(D_1 - D_2)}{3}, \\ B &= \frac{2(D_2 + D_1)}{3}, \\ \psi &= 0. \end{aligned} \quad (58)$$

In a compact form, we have

$$\begin{aligned} D_{[j]}^\alpha &= \frac{2(D_1 - D_2)}{3} \cos\left(\frac{2\pi}{3}j + \frac{2\pi}{3}(\alpha - 1)\right) + \frac{2D_2 + D_1}{3}, \\ C_{[j]}^\alpha &= \frac{2(C_1 - C_2)}{3} \cos\left(\frac{2\pi}{3}j + \frac{2\pi}{3}(\alpha - 1)\right) + \frac{2C_2 + C_1}{3}, \end{aligned} \quad (59)$$

in which  $\alpha = 1, 2, 3$  corresponding to  $x, y, z$ .

Now we are able to write the nonabelian bosonization formula with different momenta separated, *i.e.*

$$\frac{1}{a} S_i^\alpha = [c_0 + c_4 \cos\left(\frac{2\pi}{3a}x + \frac{2\pi}{3}(\alpha - 1)\right)] (J_L^\alpha(x) + J_R^\alpha(x)) [c_6 (-)^{\frac{x}{a}} + c_2 \cos\left(\frac{\pi}{3a}x + \frac{2\pi}{3}(\alpha - 1)\right)] \frac{1}{\sqrt{a}} \text{tr}(g(x)\sigma^\alpha), \quad (60)$$

in which

$$c_0 = \frac{2D_2 + D_1}{3}, c_2 = \frac{2(C_2 - C_1)}{3}, c_4 = \frac{2(D_1 - D_2)}{3}, c_6 = \frac{2C_2 + C_1}{3}. \quad (61)$$

## THE NINE- AND THREE-POINT FORMULAS

### The nine-point formula

At large distances, the uniform and the  $2\pi/3$ -oscillating components decay much faster than the staggered and the  $\pi/3$ -oscillating components. Due to this reason, we will derive a nine-point formula to extract the staggered and the  $\pi/3$ -oscillating components of the spin-spin correlation functions, assuming no uniform and the  $2\pi/3$ -oscillating components.

Let  $f(j)$  ( $j \in \mathbb{Z}$ ) be

$$f(j) = (-)^j s(j) + \cos\left(\frac{\pi}{3}j\right)p(j) + \sin\left(\frac{\pi}{3}j\right)q(j). \quad (62)$$

Write  $f(i)$  in terms of  $i - j$ , we have

$$f(i) = (-)^{i-j} s'(i - j) + \cos\left(\frac{\pi}{3}(i - j)\right)p'(i - j) + \sin\left(\frac{\pi}{3}(i - j)\right)q'(i - j), \quad (63)$$

in which

$$\begin{aligned}
s'(i-j) &= (-)^j s(i), \\
p'(i-j) &= \cos\left(\frac{\pi}{3}j\right)p(i) + \sin\left(\frac{\pi}{3}j\right)q(i), \\
q'(i-j) &= -\sin\left(\frac{\pi}{3}j\right)p(i) + \cos\left(\frac{\pi}{3}j\right)q(i).
\end{aligned} \tag{64}$$

Expanding  $s', p', q'$  as

$$\begin{aligned}
s'(k) &= s_2 k^2 + s_1 k + s_0 \\
p'(k) &= p_2 k^2 + p_1 k + p_0 \\
q'(k) &= q_2 k^2 + q_1 k + q_0,
\end{aligned} \tag{65}$$

the constants  $s_0, p_0, q_0$  can be determined as

$$\begin{aligned}
s_0 &= -\frac{1}{27}f(-4+j) + \frac{2}{27}f(-2+j) - \frac{8}{27}f(-1+j) + \frac{1}{3}f(j) - \frac{8}{27}f(1+j) + \frac{2}{27}f(2+j) - \frac{1}{27}f(4+j), \\
p_0 &= \frac{1}{27}f(-4+j) - \frac{2}{27}f(-2+j) + \frac{8}{27}f(-1+j) + \frac{2}{3}f(j) + \frac{8}{27}f(1+j) - \frac{2}{27}f(2+j) + \frac{1}{27}f(4+j), \\
q_0 &= -\frac{1}{9\sqrt{3}}f(-4+j) - \frac{2}{9\sqrt{3}}f(-2+j) - \frac{8}{9\sqrt{3}}f(-1+j) + \frac{8}{9\sqrt{3}}f(1+j) + \frac{2}{9\sqrt{3}}f(2+j) + \frac{1}{9\sqrt{3}}f(4+j).
\end{aligned} \tag{66}$$

Then  $s(j), p(j), q(j)$  can be expressed as

$$\begin{aligned}
s(j) &= (-)^j s_0 \\
p(j) &= \cos\left(\frac{\pi}{3}j\right)p_0 - \sin\left(\frac{\pi}{3}j\right)q_0 \\
q(j) &= \sin\left(\frac{\pi}{3}j\right)p_0 + \cos\left(\frac{\pi}{3}j\right)q_0.
\end{aligned} \tag{67}$$

### The three-point formula

Let  $f(j)$  ( $j \in \mathbb{Z}$ )

$$f(j) = u(j) + (-)^j s(j). \tag{68}$$

The three-point formula can be used to extract the uniform part  $u(j)$  and the stagger part  $s(j)$ , as

$$\begin{aligned}
u(j) &= \frac{1}{4}f(j-1) + \frac{1}{2}f(j) + \frac{1}{4}f(j+1), \\
s(j) &= (-)^j \left[ -\frac{1}{4}f(j-1) + \frac{1}{2}f(j) - \frac{1}{4}f(j+1) \right].
\end{aligned} \tag{69}$$

## SU(2)<sub>1</sub> CONFORMAL TOWER IN THE FINITE SIZE SPECTRUM

In this section, we study numerically the finite size spectrum of an AFM Kitaev-Gamma chain, and verify that the spectrum exhibits a conformal tower structure consistent with the emergent SU(2)<sub>1</sub> symmetry.

We first briefly review the SU(2) symmetric AFM Heisenberg point, *i.e.*,  $\phi = 5\pi/4$ , following the treatment in Ref. [4]. Due to the existence of the marginally irrelevant term  $-u\vec{J}_L \cdot \vec{J}_R$  which breaks the chiral SU(2) symmetry, the SU(2)<sub>1</sub> symmetry emerges only logarithmically along the RG flow. In particular, there is a finite size correction to the energy spectrum only suppressed by  $1/\ln L$  [5]. At small system size, the effects of such logarithmic correction are notable which obscures the emergent SU(2)<sub>1</sub> structure. However, as shown in Refs. [4, 5], there is a clever trick to get around such problem. One adds to the nearest neighbor Heisenberg Hamiltonian a next nearest neighbor  $J_2$  term, so that the Hamiltonian now becomes

$$H'_{AFM} = J \sum_n \vec{S}_n \cdot \vec{S}_{n+1} + J_2 \sum_n \vec{S}_n \cdot \vec{S}_{n+2}. \tag{70}$$

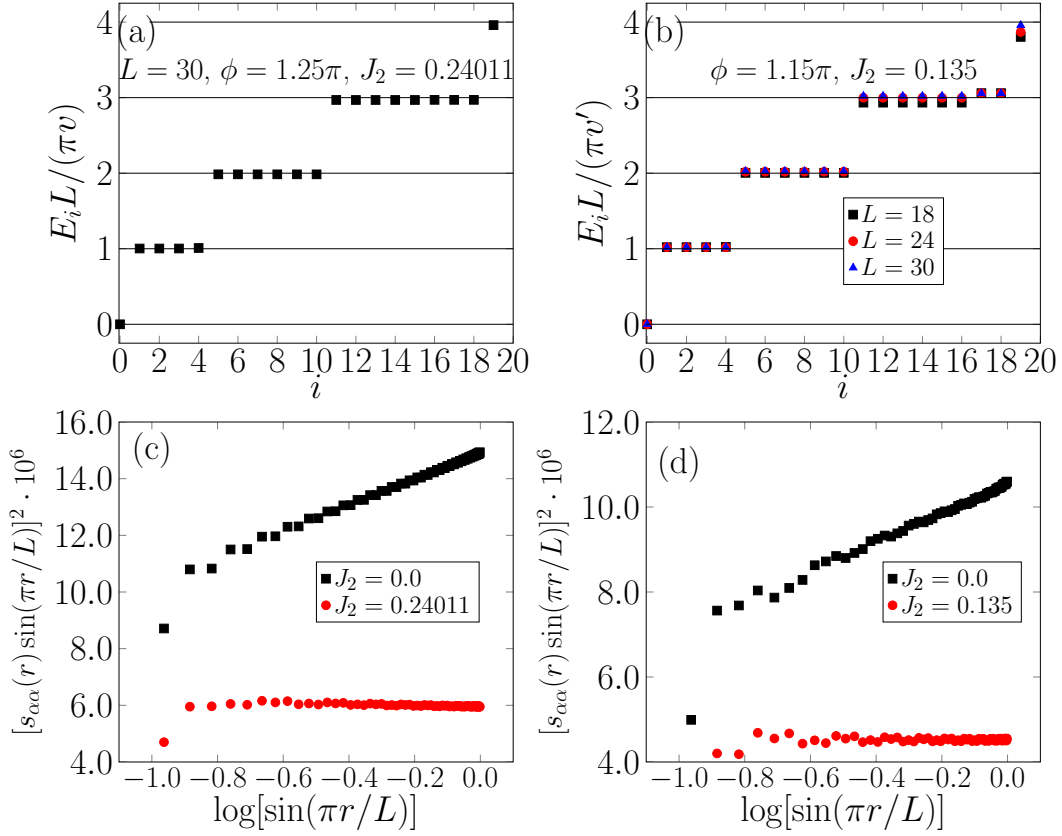


FIG. 9: Energies of the first 20 eigenstates with appropriately chosen  $J_{2c}$  for (a)  $\phi = 1.25\pi$ , and (b)  $\phi = 1.15\pi$ ; and  $(s_{\alpha\alpha}(r) \sin(\pi r/L))^2$  ( $\alpha = x$ ) vs.  $\log \sin(\pi r/L)$  with and without  $J_2$  shown by black and red dots, respectively, for (c)  $\phi = 1.25\pi$  and (d)  $\phi = 1.15\pi$ . In (a,b), the spectra are calculated using ED with a periodic boundary condition for both values of  $\phi$ . The system size is taken as  $L = 30$  for  $\phi = 1.25\pi$  in (a), and  $L = 18, 24, 30$  for  $\phi = 1.15\pi$  in (b). In (c,d), the correlation functions are computed using DMRG on a system of  $L = 144$  sites with periodic boundary conditions.  $s_{\alpha\alpha}$  is then extracted from a nine-point formula in the same way as discussed in the main text.

At certain value  $J_{2c}$ , the bare marginal operator is killed, *i.e.*,  $u' = 0$  within  $-u' \vec{J}_L \cdot \vec{J}_R$ . In fact,  $J_{2c}$  is the phase transition point between the gapless spin liquid phase and an ordered dimerized phase [4]. According to Ref. [4], when  $J_2$  is tuned to  $J_{2c} = 0.2401J$ , the finite size spectra are arranged to a nearly perfect conformal tower structure fully consistent with the  $SU(2)_1$  predictions without any logarithmic corrections. Using exact diagonalization, we have reproduced the results in Ref. [4] as shown in Fig. 9 (a), with the eigenenergies computed on a finite system with  $L = 30$  sites under periodic boundary conditions. The energies are rescaled in unit of  $\pi v/L$  where  $v = 1.1745J$ . As can be seen from Fig. 9 (a), the eigenenergies are grouped into equally spacing plateaus at  $n\pi v/L$  with  $n \in \mathbb{Z}$ . For several lowest  $n$ 's, the degeneracies are: 4 for  $n = 1$ , 6 for  $n = 2$ , 8 for  $n = 3$ , all consistent with the emergent  $SU(2)_1$  symmetry.

To confirm the absence of the marginal operator  $-u' \vec{J}_L \cdot \vec{J}_R$  at  $J_{2c}$ , we further calculate the spin-spin correlation function  $\langle S_1^\alpha S_{r+1}^\alpha \rangle$  ( $\alpha = x$ ) using DMRG on a system of a size  $L = 144$  with a periodic boundary condition. We stress that, although it is well known that DMRG simulations are more challenging in the presence of periodic boundary conditions, these were only used to demonstrate evidence for the logarithmic corrections predicted by the bosonization expression in the main text. Our analysis indeed shows that system sizes of the order of  $\sim 150$  sites are sufficient for this purpose. To reach numerical convergence in the presence of PBC, up to  $m = 1000$  DMRG states were kept and tens of finite size sweeps were performed with a final truncation error of  $10^{-6}$ . Since the momentum  $\pi$  and  $\pm\pi/3$  components decay as  $1/r$  at long distances which dominates over the momentum 0 and  $\pm 2\pi/3$  components which decay as  $1/r^2$ , we will assume that  $\langle S_1^\alpha S_{r+1}^\alpha \rangle$  only contains the  $\pi$  and  $\pm\pi/3$  oscillating components. Then the nine-point formula can be applied and the staggered part  $s_{\alpha\alpha}(r)$  can be extracted which should behave as  $\sim 1/\sin(\pi r/L)$  with no logarithmic factor. Indeed, as shown by the red points in Fig. 9 (c),  $(s_{\alpha\alpha}(r) \sin(\pi r/L))^2$  vs.  $\log(\sin(\pi r/L))$  is nearly a flat line consistent with an absence of the logarithmic factor. On the other hand, the black dots show

the results of  $(s_{\alpha\alpha}(r) \sin(\pi r/L))^2$  vs.  $\log(\sin(\pi r/L))$  when  $J_2 = 0$ . The linear relation of the black dots indicates a behavior of  $s_{\alpha\alpha}(r)$  as  $\sim \ln^{1/2}(\sin(\pi r/L))/\sin(\pi r/L)$ . Hence, this provides evidence for the role of  $J_{2c}$  in killing the marginal operator.

Next we apply the same methods to a representative point  $\phi = 1.15\pi$  away from the  $SU(2)$  symmetric point. Again by adding a  $J_2$  term, the Hamiltonian now is

$$H'_{K\Gamma} = -J \sum_{\langle ij \rangle \in \gamma} [\cos(\phi) S_i^\gamma S_j^\gamma + \sin(\phi)(S_i^\alpha S_j^\alpha + S_i^\beta S_j^\beta)] + J_2 \sum_n \vec{S}_n \cdot \vec{S}_{n+2}. \quad (71)$$

In Fig. 9 (d),  $(s_{\alpha\alpha}(r) \sin(\pi r/L))^2$  vs.  $\log(\sin(\pi r/L))$  at  $J_2 = 0$  are plotted with black dots showing a linear relation with a nonzero slope. On the other hand, the slope is zero when  $J_2 = 0.135J$  as can be seen from the red dots. Thus, this time the critical  $J'_{2c}$  is  $0.135J$  which is able to remove the marginal operator  $-u\vec{J}_L \cdot \vec{J}_R$  in the low energy theory. In Fig. 9 (b), the energies of the first 20 states are plotted for  $L = 18, 24, 30$  in units of  $\pi v'/L$ . Here  $v' = 0.6479J$  is determined by an extrapolation of  $E_1(L) - E_0(L)$  as a function of  $1/L$  to  $1/L \rightarrow 0$ , in which  $E_0(L)$  and  $E_1(L)$  are the energies of the ground state and the first excited state, respectively. As can be seen from Fig. 9 (b), the  $SU(2)_1$  conformal tower structure in the finite size spectrum is improved by increasing  $L$ . And in fact, a good agreement with the  $SU(2)$  symmetric case in Fig. 9 (a) is already obtained when  $L = 30$ . This provides strong evidence for the emergent  $SU(2)_1$  symmetry at low energies even away from  $\phi = 1.25\pi$ .

## RG FLOWS OF THE SCALING FIELDS

### Derivation of the RG flow equations

Conceptually, the RG flow of the theory described by the following Hamiltonian (*i.e.*,  $H_F$  in the maintext)

$$H_F = -t \sum_{\langle ij \rangle, \alpha} (c_{i\alpha}^\dagger c_{j\alpha} + \text{h.c.}) - \mu \sum_{i\alpha} c_{i\alpha}^\dagger c_{i\alpha} + U \sum_i n_{i\uparrow} n_{i\downarrow} + \Delta \sum_{\langle ij \rangle \in \gamma} S_i^\gamma S_j^\gamma - \sum_{kn\alpha} h_k^\alpha(n) S_{k+3n}^\alpha \quad (72)$$

can be separated into three steps,

$$\Lambda_0 \rightarrow \Lambda_1 \rightarrow \Lambda_2 \rightarrow E(\gg \frac{1}{L}), \quad (73)$$

where  $\Lambda_0 = \pi/a$  is the bare cutoff,  $\Lambda_1$  is the energy scale at which the three sites within a unit cell get smeared,  $\Lambda_2$  is the energy scale at which a linearization of the free fermion dispersion applies, and  $1/E$  is the length scale of the correlation functions. Below the energy scale  $\Lambda_2$ , the fermion becomes a Dirac fermion and can be written alternatively in terms of a charge boson and an  $SU(2)$  WZW boson using nonabelian bosonization. However, now we study the flow in the energy region  $\Lambda_0 \rightarrow \Lambda_1$ .

We first give a heuristic argument to the RG flow equations based on the operator product expansion (OPE) in real space. The origin of the multiplicative renormalizations of the scaling fields is clear in this approach. However, the OPE approach is not rigorous since it only applies to the continuum limit, and now the flow is within the high energy region. Later we will derive the RG flow in a more rigorous manner in the framework of Wilsonian momentum shell RG.

First recall how the RG flow can be obtained from the OPE between operators [6]. Let  $\sum_i g_i \hat{O}_i$  be in the Hamiltonian, in which  $\hat{O}_i$  is an operator with scaling dimension  $x_i$ . If the OPEs between  $\hat{O}_i$ 's are given by

$$\hat{O}_i(x) \hat{O}_j(y) \sim \frac{c_{ijk}}{|x-y|^{x_i+x_j-x_k}} \hat{O}_k(\frac{x+y}{2}), \quad (74)$$

then the flow for the coupling  $g_k$  up to one-loop level is

$$\frac{dg_k}{d \ln b} = (d - x_i)g_k - \frac{1}{2} S_d c_{ijk} g_i g_j, \quad (75)$$

in which  $x, y$  are spacetime coordinates,  $d$  is the spacetime dimension, and  $S_d = (2\pi)^{d/2}/\Gamma(d/2)$  is the solid angle of the  $(d-1)$ -dimensional unit sphere. In our case, take  $h_{u,1}^x$  as an example. Heuristically, if we take the discrete

unit cell index  $n$  as a continuous variable, and combine  $n$  with  $\tau$  into  $x = (\tau, n)$ , then we obtain the following OPE ( $j = 1, 2, 3$ ),

$$S_1^x(x)S_2^x(x) \cdot S_j^x(y) \sim \langle S_2^x(x)S_j^x(y) \rangle S_1^x(x). \quad (76)$$

Hence  $h_{u,j}^x$  ( $j = 1, 2, 3$ ) all contribute to the renormalization of  $h_{u,1}^x$ . The RG flow equation is then

$$\frac{dh_{u,1}^x}{d \ln b} = (1 - \lambda_{21}\Delta)h_{u,1}^x - \lambda_{22}\Delta h_{u,2}^x - \lambda_{23}\Delta h_{u,3}^x, \quad (77)$$

in which  $\lambda_{2j}$  is determined by the contraction  $\langle S_2^x(x)S_j^x(y) \rangle$ . Furthermore,  $\lambda_{21} = \lambda_{23}$  due to the inversion symmetry of the free fermion band structure. In addition, from a simple argument we expect that  $\lambda_{22} > \lambda_{23} = \lambda_{21}$ . This is because at short distances the  $j = 2$  contraction in Eq. (76) contains less oscillation than the  $j = 1, 3$  cases, since at  $x = y$ , the  $j = 2$  contraction is on-site while the  $j = 1, 3$  terms are off-site. Thus we are able to obtain the form of the RG equations presented in the main text in a simple manner, and even the relation  $\lambda > 0 > \nu$  is expected. For the staggered part  $h_{s,i}^\alpha$ , roughly speaking, one needs to change  $\Delta$  to  $-\Delta$  since the spin operators on two adjacent sites differ by a sign. Thus the slope of  $C_2/C_1$  and  $D_2/D_1$  around  $\phi = \phi_{AF}$  should be opposite in sign.

In what follows, the flows of  $h_{u,i}^\alpha$  and  $h_{s,i}^\alpha$  will be considered in a momentum shell RG approach. The signs and the magnitudes of the coefficients  $\lambda_j$ 's will be determined. We will neglect the flows of  $U$  and  $\Delta$  since they are marginal near the free fermion fixed point and the RG stopping scale  $b_1 \sim 3$  is not very large. We also ignore the contribution from  $U$  to the flows of the scaling fields, since this contribution is SU(2) symmetric.

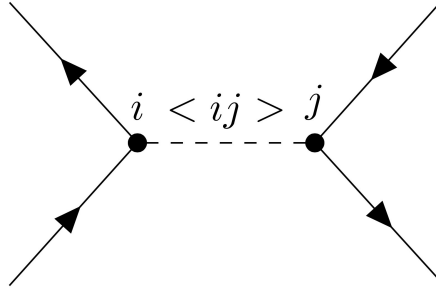


FIG. 10: Interaction vertex for the SU(2) breaking  $\Delta$ -term.

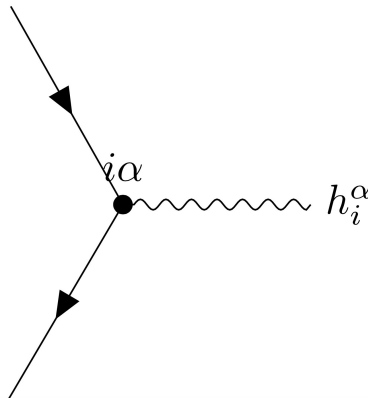


FIG. 11: Vertex for the scaling fields.

Now we proceed to a momentum shell RG treatment. Let's first write the terms within the action in the frequency-momentum space. The  $\Delta$ -term is represented as the diagram in Fig. 10, in which  $i, j = 1, 2, 3$ , and  $\langle ij \rangle = x, z, y$  for the bonds  $\langle 12 \rangle, \langle 23 \rangle, \langle 31 \rangle$ . In the frequency-momentum space, the expression corresponding to Fig. 10 is

(denoting  $\langle ij \rangle$  as  $\gamma$  for short)

$$\begin{aligned}
& \Delta \int d\tau \sum_n S_i^\gamma(\tau, n) S_j^\gamma(\tau, n) \\
&= \Delta \int d\tau \sum_n S^\gamma(\tau, i + 3n) S^\gamma(\tau, j + 3n) \\
&= \frac{\Delta}{N\beta} \int d\tau \sum_n \sum_{k_1, k_2, k_3, k_4} c^\dagger(k_1) \frac{1}{2} \sigma^\gamma c(k_2) \cdot c^\dagger(k_3) \frac{1}{2} \sigma^\gamma c(k_4) e^{i(\omega_1 - \omega_2 + \omega_3 - \omega_4)\tau} e^{i(\vec{k}_1 - \vec{k}_2)(i+3n)a\hat{x}} e^{i(\vec{k}_3 - \vec{k}_4)(j+3n)a\hat{x}}, \quad (78)
\end{aligned}$$

in which  $k = (i\omega, \vec{k})$ ,  $a$  is the lattice spacing,  $N$  is the total number of sites,  $\beta$  is the inverse of temperature,  $n$  is summed over the unit cells, and  $\hat{x}$  is the unit vector in the spatial direction. By integrating over  $\tau$  and summing over  $n$ , and using

$$\frac{1}{N} \sum_n e^{i(\vec{k}_1 - \vec{k}_2 + \vec{k}_3 - \vec{k}_4) \cdot 3na\hat{x}} = \frac{1}{3} \sum_{m=1}^3 \delta_{\vec{k}_1 - \vec{k}_2 + \vec{k}_3 - \vec{k}_4, \frac{2\pi}{3a} m\hat{x}}, \quad (79)$$

Eq. (78) is equal to

$$\frac{\Delta}{N\beta} \frac{1}{3} \sum_m \sum_{k_1, k_2, k_3, k_4} e^{i(\vec{k}_1 - \vec{k}_2)(i-j)a\hat{x}} e^{-i\frac{2\pi}{3}mj} \delta_{k_1 - k_2 + k_3 - k_4 + \frac{2\pi}{3a}m\hat{x}, 0} c^\dagger(k_1) \frac{1}{2} \sigma^\gamma c(k_2) \cdot c^\dagger(k_3) \frac{1}{2} \sigma^\gamma c(k_4). \quad (80)$$

Hence we obtain

$$\Delta \int d\tau \sum_n S_i^\gamma(\tau, n) S_j^\gamma(\tau, n) = \Delta \frac{1}{3N\beta} \sum_m e^{-i\frac{2\pi}{3}mj} \sum_{k,p,q} e^{i\vec{q} \cdot (i-j)a\hat{x}} c^\dagger(k+q) \frac{1}{2} \sigma^\gamma c(k) \cdot c^\dagger(p-q) \frac{1}{2} \sigma^\gamma c(p + \frac{2\pi}{3a}m\hat{x}). \quad (81)$$

The magnetic field term is represented as the diagram in Fig. 11. The expression in the frequency-momentum space is

$$\begin{aligned}
& \int d\tau \sum_n h_l^\alpha(\tau, n) S_l^\alpha(\tau, n) \\
&= \int d\tau \sum_n h_l^\alpha(\tau, n) S^\alpha(\tau, l + 3n) \\
&= \int d\tau \sum_n \frac{1}{N\beta} \sum_q h_l^\alpha(-q) e^{-i\omega\tau} e^{-i\vec{q} \cdot 3na\hat{x}} \sum_{q'} S^\alpha(q') e^{i\omega\tau} e^{i\vec{q}' \cdot (l+3n)a\hat{x}} \\
&= \frac{1}{3} \sum_q \sum_m e^{i\vec{q} \cdot la\hat{x}} e^{i\frac{2\pi}{3}ml} h_l^\alpha(-q) S^\alpha(q + \frac{2\pi}{3a}m\hat{x}). \quad (82)
\end{aligned}$$

In terms of the fermion operators, we have

$$\int d\tau \sum_n h_l^\alpha(\tau, n) S_l^\alpha(\tau, n) = \frac{1}{3} \sum_{kq} \sum_m e^{i\vec{q} \cdot la\hat{x}} e^{i\frac{2\pi}{3}ml} h_l^\alpha(-q) c^\dagger(k + \frac{2\pi}{3a}m\hat{x}) \frac{1}{2} \sigma^\alpha c(k - q), \quad (83)$$

in which  $c^\dagger(k) = (c_\uparrow^\dagger(k), c_\downarrow^\dagger(k))$ . In what follows, we focus on the uniform part  $h_{u,i}^\alpha(\tau, n)$ . Then the momentum transfer  $\vec{q}$  is  $|\vec{q}| \sim 0$ . If we want to consider the staggered part  $h_{s,i}^\alpha$ , we should write  $\vec{q} = \vec{q}' + \pi/3$ , with  $|\vec{q}'| \sim 0$ .

Next we consider the renormalization of  $h_{u,i}^\alpha$  due to the effect of the  $\Delta$ -term. In what follows, we will drop the subscript ‘‘u’’ for simplicity. The diagram is shown in Fig. 12 in which the momentum integrated within the loop corresponds to the fast mode (represented as  $>$  in the figure) in the treatment of a momentum shell RG. Take the renormalization of  $h_1^x$  as an example. Notice that the term  $\Delta \int d\tau \sum_n S_{1+3n}^x(\tau) S_{2+3n}^x(\tau)$  contributes to the renormalization of  $h_1^x$  by contracting  $S_{2+3n}^x(\tau)$  with  $S_{l+3n'}^x(\tau')$  ( $l = 1, 2, 3$ ). Thus in Fig. 12, we should make the substitution  $i \rightarrow 1, j \rightarrow 2, l \rightarrow l$ .

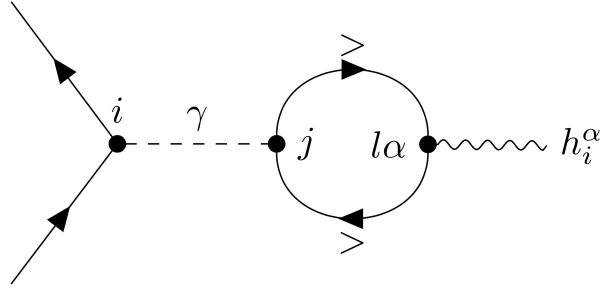


FIG. 12: Diagram of the renormalization of the scaling fields due to the SU(2) breaking  $\Delta$ -term.

The analytic expression corresponding to Fig. 12 is

$$\begin{aligned} & \Delta \frac{1}{3N\beta} \sum_m e^{-i\frac{2\pi}{3a}mj} \sum_{kpq} e^{i\vec{q}\cdot(i-j)a\hat{x}} c^\dagger(k+q) \frac{1}{2} \sigma^\gamma c(k) \cdot \frac{1}{3} \sum_{k'q'm'} e^{i\vec{q}'\cdot la\hat{x}} e^{i\frac{2\pi}{3}m'l} h_l^\alpha(-q') \\ & \times \langle c^\dagger(p-q) \frac{1}{2} \sigma^\gamma c(p + \frac{2\pi}{3a}m\hat{x}) c^\dagger(k' + \frac{2\pi}{3a}m'\hat{x}) \frac{1}{2} \sigma^\alpha c(\vec{k}' - q') \rangle_f, \end{aligned} \quad (84)$$

in which  $\langle \rangle_f$  represents averaging over fast modes. The averaging leads to the following momentum constraints,

$$\begin{aligned} p + \frac{2\pi}{3a}m &= k' + \frac{2\pi}{3a}m', \\ p - q &= k' - q', \end{aligned} \quad (85)$$

which gives

$$\begin{aligned} m' &= m + \bar{m} \\ p &= k' + \frac{2\pi}{3a}\bar{m} \\ q &= q' + \frac{2\pi}{3a}\bar{m}, \end{aligned} \quad (86)$$

in which  $\bar{m} = 1, 2, 3$ . Then Eq. (84) becomes

$$\begin{aligned} & \Delta \frac{1}{9N\beta} \sum_{m,\bar{m}} \sum_{kk'q'} e^{-i\frac{2\pi}{3a}mj} e^{i\vec{q}'\cdot(i-j)a\hat{x}} e^{i\frac{2\pi}{3}\bar{m}(i-j)} e^{i\vec{q}'\cdot la\hat{x}} e^{i\frac{2\pi}{3}(m+\bar{m})l} h_l^\alpha(-q') c^\dagger(k+q' + \frac{2\pi}{3a}\bar{m}\hat{x}) \frac{1}{2} \sigma^\gamma c(k) \\ & \times \langle c^\dagger(k' - q') \frac{1}{2} \sigma^\gamma c(k' + \frac{2\pi}{3a}(m+\bar{m})\hat{x}) c^\dagger(k' + \frac{2\pi}{3a}(m+\bar{m})\hat{x}) \frac{1}{2} \sigma^\alpha c(\vec{k}' - q') \rangle_f. \end{aligned} \quad (87)$$

To further simplify the expression,  $e^{-i\frac{2\pi}{3a}mj}$  and  $e^{-i\frac{2\pi}{3}\bar{m}j}$  are first collected together, then combined with  $e^{i\frac{2\pi}{3}(m+\bar{m})l}$ . The combined factor is then put together with the  $\langle \rangle_f$  term and the result depends on  $m + \bar{m}$  only. The remaining terms only depend on  $\bar{m}$ . Doing these, we obtain

$$\begin{aligned} & \frac{1}{3} \sum_{\bar{m}} e^{i\frac{2\pi}{3a}\bar{m}i} \sum_{kq'} e^{i\vec{q}'\cdot ia\hat{x}} h_l^\alpha(-q') c^\dagger(k+q' + \frac{2\pi}{3a}\bar{m}\hat{x}) \frac{1}{2} \sigma^\gamma c(k) \\ & \times \frac{\Delta}{3N\beta} e^{-i\vec{q}'\cdot(j-l)a\hat{x}} \sum_m \sum_{k'} e^{-i\frac{2\pi}{3}(m+\bar{m})(j-l)} \langle c^\dagger(k' - q') \frac{1}{2} \sigma^\gamma c(k + \frac{2\pi}{3a}(m+\bar{m})\hat{x}) c^\dagger(k' + \frac{2\pi}{3a}(m+\bar{m})\hat{x}) \frac{1}{2} \sigma^\alpha c(\vec{k}' - q') \rangle_f. \end{aligned} \quad (88)$$

Notice that in Eq. (88), the average  $\langle \rangle_f$  is non-vanishing only when  $\alpha = \gamma$ . Hence the first line in Eq. (88) is simply  $\int d\tau \sum_n h_l^\alpha(\tau, n) S_l^\alpha(\tau, n)$  as can be seen from Eq. (83). This confirms that the diagram in Fig. 12 indeed renormalizes  $h_i^\alpha$ . Since  $q'$  is a slow wavevector, we can ignore  $q'$  in the remaining part of Eq. (88) other than the field term. In summary, we conclude that Eq. (88) is equal to

$$\Delta \lambda_{jl} \delta_{\alpha\gamma} \ln b \cdot \int d\tau \sum_n h_l^\alpha(\tau, n) S_l^\alpha(\tau, n). \quad (89)$$

The coefficient is

$$\lambda_{jl} \ln b = -\frac{a}{6} \sum_m e^{-i\frac{2\pi}{3}m(j-l)} \int_{\Lambda/b}^{\Lambda} d^2k \mathcal{G}(k) \mathcal{G}(k + \frac{2\pi}{3a}m\hat{x}), \quad (90)$$

in which at zero temperature the sum over  $k'$  is turned into an integral restricted within the momentum shell  $[\Lambda/b, \Lambda]$ , “ $a$ ” is the lattice constant, the minus sign comes from the fermion loop, and

$$\mathcal{G}(k) = \frac{1}{i\omega - \epsilon(k)} \quad (91)$$

is the free fermion Green’s function where  $\epsilon(k)$  is the dispersion. In conclusion, the RG flow equation for the scaling field is

$$\frac{dh_{u,i}^\alpha}{d \ln b} = h_{u,i}^\alpha - \lambda_{jl} \Delta h_{u,l}^\alpha, \quad (92)$$

in which  $\alpha = \langle ij \rangle$ .

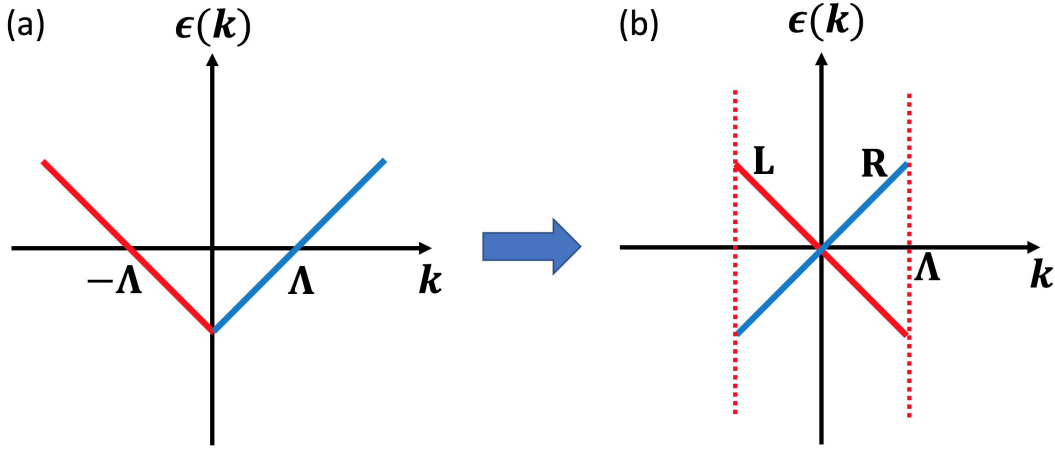


FIG. 13: Free fermion fixed point dispersion.

Next we proceed to calculating the coefficients  $\lambda_{jl}$  in the flow equations. At the free fermion fixed point, the dispersion is linear as shown in Fig. 13 (a). We ignore the nonlinear terms in the band structure since they are of higher dimensions hence irrelevant in the vicinity of the free fermion fixed point. The dispersion can be folded into a Dirac fermion with left and right movers as shown in Fig. 13 (a), in which the cutoff  $\Lambda = \frac{\pi}{2a}$ .

In momentum shell RG, the modes  $(\omega, \vec{k})$  satisfying  $\sqrt{\omega^2 + (v\vec{k})^2} \in [\Lambda/b, \Lambda]$  are integrated over, where  $v = ta$  is the free fermion velocity and  $t$  is the hopping strength. By rescaling  $(\omega, \vec{k})$  to  $(\omega/(v\Lambda), \vec{k}/\Lambda)$ , Eq. (90) becomes

$$\lambda_{jl} \ln b = -\frac{1}{6t} \sum_m e^{-i\frac{2\pi}{3}m(j-l)} \ln b \sum_{\nu=\pm 1} \int \frac{d\theta}{4\pi^2} \frac{1}{i \cos \theta - \bar{\epsilon}(\sin \theta + \nu)} \frac{1}{i \cos \theta - \bar{\epsilon}(\sin \theta + \nu + \frac{4}{3}m)}, \quad (93)$$

in which  $\nu = \pm 1$  corresponds to left and right movers, and  $\bar{\epsilon}(x) = \text{sgn}(x) - 1$ ,  $-2 \leq x \leq 2$  ( $x$  is mod 4). Thus

$$\begin{aligned} \lambda_{jl} &= \frac{1}{24\pi^2 t} \sum_{m=0, \pm 1} e^{-i\frac{2\pi}{3}m(j-l)} \sum_{\nu=\pm 1} \int_0^{2\pi} d\theta \frac{1}{\cos^2 \theta + \bar{\epsilon}^2(\sin \theta + \nu)} \frac{1}{\cos^2 \theta + \bar{\epsilon}^2(\sin \theta + \nu + \frac{4}{3}m)} \\ &\times \left[ \cos^2 \theta - \bar{\epsilon}(\sin \theta + \nu) \bar{\epsilon}(\sin \theta + \nu + \frac{4}{3}m) - i \cos \theta (\bar{\epsilon}(\sin \theta + \nu) + \bar{\epsilon}(\sin \theta + \nu + \frac{4}{3}m)) \right]. \end{aligned} \quad (94)$$

The imaginary part vanishes, as can be seen by performing a change of variable  $\theta \rightarrow \pi - \theta$  under which  $\sin \theta$  is invariant but  $\cos \theta$  changes a sign. The  $m = 0$  term also vanishes. This is because the  $\theta$ -integral for both the left and right movers is equal to  $\int d\theta (\cos^2 \theta - \sin^2 \theta) = 0$ . Thus we obtain

$$\lambda_{jl} = \frac{1}{24\pi^2 t} \sum_{m=\pm 1} e^{-i\frac{2\pi}{3}m(j-l)} \sum_{\nu=\pm 1} \int_0^{2\pi} d\theta \frac{\cos^2 \theta - \bar{\epsilon}(\sin \theta + \nu) \bar{\epsilon}(\sin \theta + \nu + \frac{4}{3}m)}{[\cos^2 \theta + \bar{\epsilon}^2(\sin \theta + \nu)] \cdot [\cos^2 \theta + \bar{\epsilon}^2(\sin \theta + \nu + \frac{4}{3}m)]}. \quad (95)$$

Using  $\bar{\epsilon}(x) = \bar{\epsilon}(-x)$ , it can be further shown that in Eq. (95),  $(m = 1, \nu = 1)$  is equal to  $(m = -1, \nu = -1)$ , and  $(m = 1, \nu = -1)$  is equal to  $(m = -1, \nu = 1)$ . Hence we get

$$\lambda_{jl} = \frac{1}{t} E \cos\left(\frac{2\pi}{3}(j-l)\right), \quad (96)$$

in which

$$E = \frac{1}{12\pi^2} \sum_{\nu=\pm 1} \int_0^{2\pi} d\theta \frac{\cos^2 \theta - \bar{\epsilon}(\sin \theta + \nu) \bar{\epsilon}(\sin \theta + \nu + \frac{4}{3})}{[\cos^2 \theta + \bar{\epsilon}^2(\sin \theta + \nu)] \cdot [\cos^2 \theta + \bar{\epsilon}^2(\sin \theta + \nu + \frac{4}{3})]}. \quad (97)$$

The numerical evaluation of  $E$  gives  $E = 0.14$ .

The flow equation of  $h_1^x$  now becomes

$$\begin{aligned} \frac{dh_{u,1}^x}{d \ln b} &= h_{u,1}^x - \lambda_{22} \Delta h_{u,2}^x - \lambda_{23} \Delta h_{u,3}^x \\ &= h_{u,1}^x - E \frac{\Delta}{t} h_{u,2}^x - E \cos\left(\frac{2\pi}{3}\right) \frac{\Delta}{t} h_{u,3}^x. \end{aligned} \quad (98)$$

Comparing with the flow equation in the main text, we see that

$$\begin{aligned} \lambda &= \frac{1}{t} E > 0, \\ \nu &= \frac{1}{t} E \cos\left(\frac{2\pi}{3}\right) < 0. \end{aligned} \quad (99)$$

Finally we discuss the flow of the staggered part  $h_{s,i}^\alpha$ . We give a quick derivation for the flow equation of  $h_{s,i}^\alpha$ , only highlighting the difference from the derivation for the flow of the uniform part.

By replacing  $h_l^\alpha(\tau, n)$  by  $(-)^n h_{s,l}^\alpha(\tau, n)$  in Eq. (83), we obtain

$$\int d\tau \sum_n h_l^\alpha(\tau, n) S_l^\alpha(\tau, n) = \frac{1}{3} \sum_{kq} \sum_m e^{i\vec{q} \cdot l a \hat{x}} e^{i\frac{2\pi}{3}(m+\frac{1}{2})l} (-)^l h_{s,l}^\alpha(-q) c^\dagger(k + \frac{2\pi}{3a} m \hat{x} + \frac{\pi}{3a} \hat{x}) \frac{1}{2} \sigma^\alpha c(k-q). \quad (100)$$

In what follows, we will drop the subscript ‘‘s’’ for simplicity. The renormalization expression in Eq. (84) becomes

$$\begin{aligned} &\Delta \frac{1}{3N\beta} \sum_m e^{-i\frac{2\pi}{3a} m j} \sum_{kpq} e^{i\vec{q}' \cdot (i-j) a \hat{x}} c^\dagger(k+q) \frac{1}{2} \sigma^\gamma c(k) \cdot \frac{1}{3} \sum_{k'q'm'} e^{i\vec{q}' \cdot l a \hat{x}} e^{i\frac{2\pi}{3}(m'+\frac{1}{2})l} (-)^l h_l^\alpha(-\vec{q}') \\ &\times \langle c^\dagger(p-q) \frac{1}{2} \sigma^\gamma c(p + \frac{2\pi}{3a} m \hat{x}) c^\dagger(k' + \frac{2\pi}{3a} m' \hat{x} + \frac{\pi}{3a} \hat{x}) \frac{1}{2} \sigma^\alpha c(\vec{k}' - q') \rangle_f, \end{aligned} \quad (101)$$

and the momentum conservations in Eq. (86) are now

$$\begin{aligned} m' &= m + \bar{m} \\ p &= k' + \frac{2\pi}{3a} \bar{m} + \frac{\pi}{3a} \\ q &= q' + \frac{2\pi}{3a} \bar{m} + \frac{\pi}{3a}. \end{aligned} \quad (102)$$

Then Eq. (103) becomes

$$\begin{aligned} &\frac{1}{3} \sum_{\bar{m}} e^{i\frac{2\pi}{3a}(\bar{m}+\frac{1}{2})i} (-)^i \sum_{kq'} e^{i\vec{q}' \cdot i a \hat{x}} h_l^\alpha(-q') c^\dagger(k+q' + \frac{2\pi}{3a} \bar{m} \hat{x}) \frac{1}{2} \sigma^\gamma c(k) \times \frac{\Delta}{3N\beta} e^{-i\vec{q}' \cdot (j-l) a \hat{x}} (-)^{i-l} \\ &\cdot \sum_m \sum_{k'} e^{-i\frac{2\pi}{3}(m+\bar{m}+\frac{1}{2})(j-l)} \langle c^\dagger(k' - q') \frac{1}{2} \sigma^\gamma c(k + \frac{2\pi}{3a} (m + \bar{m} + \frac{1}{2}) \hat{x}) c^\dagger(k' + \frac{2\pi}{3a} (m + \bar{m} + \frac{1}{2}) \hat{x}) \frac{1}{2} \sigma^\alpha c(\vec{k}' - q') \rangle_f. \end{aligned} \quad (103)$$

Instead of Eq. (90), Eq. (103) leads to an RG coefficient

$$\lambda_{jl} \ln b = -\frac{a}{6} (-)^{i-l} \sum_m e^{-i\frac{2\pi}{3}(m+\frac{1}{2})(j-l)} \int_{\Lambda/b}^\Lambda d^2 k \mathcal{G}(k) \mathcal{G}(k + \frac{2\pi}{3a} (m + \frac{1}{2}) \hat{x}). \quad (104)$$

Correspondingly, Eq. (95) is changed to

$$\lambda_{jl} = \frac{1}{24\pi^2 t} (-)^{i-l} \sum_{m=0, \pm 1} e^{-i\frac{2\pi}{3}(m+\frac{1}{2})(j-l)} \sum_{\nu=\pm 1} \int_0^{2\pi} d\theta \frac{\cos^2 \theta - \bar{\epsilon}(\sin \theta + \nu) \bar{\epsilon}(\sin \theta + \nu + \frac{4}{3}(m+\frac{1}{2}))}{[\cos^2 \theta + \bar{\epsilon}^2(\sin \theta + \nu)] \cdot [\cos^2 \theta + \bar{\epsilon}^2(\sin \theta + \nu + \frac{4}{3}(m+\frac{1}{2}))]}, \quad (105)$$

where in particular, the  $m = 0$  term does not vanish in the current situation. Define  $E_m$  as

$$E_m = \frac{1}{24\pi^2} \sum_{\nu=\pm 1} \int_0^{2\pi} d\theta \frac{\cos^2 \theta - \bar{\epsilon}(\sin \theta + \nu) \bar{\epsilon}(\sin \theta + \nu + \frac{4}{3}(m+\frac{1}{2}))}{[\cos^2 \theta + \bar{\epsilon}^2(\sin \theta + \nu)] \cdot [\cos^2 \theta + \bar{\epsilon}^2(\sin \theta + \nu + \frac{4}{3}(m+\frac{1}{2}))]}, \quad (106)$$

we have

$$\lambda_{jl} = \frac{1}{t} (-)^{i-l} \sum_{m=0, \pm 1} e^{-i\frac{2\pi}{3}(m+\frac{1}{2})(j-l)} E_m. \quad (107)$$

The values of  $E_m$  can be evaluated numerically as

$$E_0 = -0.069, E_{+1} = 0.053, E_{-1} = -0.069. \quad (108)$$

Notice that  $\lambda_{jl}$  only depends on  $j - l$ , where  $j - l = 0, \pm 1 \pmod 3$ . It is straightforward to obtain  $\lambda_{ii} = -0.039/t$ ,  $\lambda_{i, i\pm 1} = 0.060/t$ .

### Solving the flow equations

In this section, we solve the flow equations

$$\begin{aligned} \frac{dh_1^x}{dt} &= (1 - \nu\Delta)h_1^x - \lambda\Delta h_2^x - \nu\Delta h_3^x, \\ \frac{dh_2^x}{dt} &= (1 - \nu\Delta)h_2^x - \lambda\Delta h_1^x - \nu\Delta h_3^x, \\ \frac{dh_3^x}{dt} &= h_3^x, \end{aligned} \quad (109)$$

in which  $t = \ln b$ , and the subscripts  $u, s$  are dropped in  $h$  for simplicity. The initial conditions are  $h_j^x(t=0) = h_j^x(0)$ ,  $j = 1, 2, 3$ .

The equation for  $h_3^x(t)$  is easily solved as

$$h_3^x(t) = e^t h_3^x(0). \quad (110)$$

The sum and difference of the equations for  $h_1^x, h_2^x$  are

$$\begin{aligned} \frac{d(h_1^x + h_2^x)}{dt} &= (1 - (\nu + \lambda)\Delta)(h_1^x + h_2^x) - 2\nu\Delta h_3^x, \\ \frac{d(h_1^x - h_2^x)}{dt} &= (1 - (\nu - \lambda)\Delta)(h_1^x - h_2^x). \end{aligned} \quad (111)$$

The second equation in Eq. (111) can be readily solved as

$$h_1^x(t) - h_2^x(t) = e^{(1-(\nu-\lambda)\Delta)t} (h_1^x(0) - h_2^x(0)). \quad (112)$$

To solve the first equation in Eq. (111), let

$$h_1^x(t) + h_2^x(t) = u(t)e^{(1-(\nu+\lambda)\Delta)t}. \quad (113)$$

The equation for  $u(t)$  is

$$\frac{du}{dt} = -2\nu\Delta h_3^x(0)e^{(\lambda+\nu)\Delta t}, \quad (114)$$

which can be solved as

$$u(t) = h_1^x(0) + h_2^x(0) + \frac{2\nu}{\nu+\lambda} h_3^x(0)(1 - e^{(\nu+\lambda)\Delta t}). \quad (115)$$

Keeping terms only up to first order in  $\Delta$ , we get

$$\begin{aligned} h_1^x(b) &= b[(1 - \nu\Delta \ln b)h_1^x(0) - \lambda\Delta \ln b h_2^x(0) - \nu\Delta \ln b h_3^x(0)], \\ h_2^x(b) &= b[(1 - \nu\Delta \ln b)h_2^x(0) - \lambda\Delta \ln b h_1^x(0) - \nu\Delta \ln b h_3^x(0)], \\ h_3^x(b) &= b h_3^x(0). \end{aligned} \quad (116)$$

## MORE ON AFM PHASE

### DMRG numerics

Our numerics show that periodic boundary conditions (PBC) are more efficient than open boundary conditions (OBC) in demonstrating the  $1/r^2$  behavior and the logarithmic corrections. We stress that although DMRG simulations are more challenging with PBC, in the AFM phase a choice of  $L = 144$  sites with PBC is sufficient for the purpose of demonstrating the modified nonabelian bosonization formula. To reach numerical convergence, up to  $m = 1000$  DMRG states were kept and tens of finite size sweeps were performed with a truncation error of  $10^{-6}$ .

#### Numerical study on the $\pi/3$ -oscillating components of the correlation functions

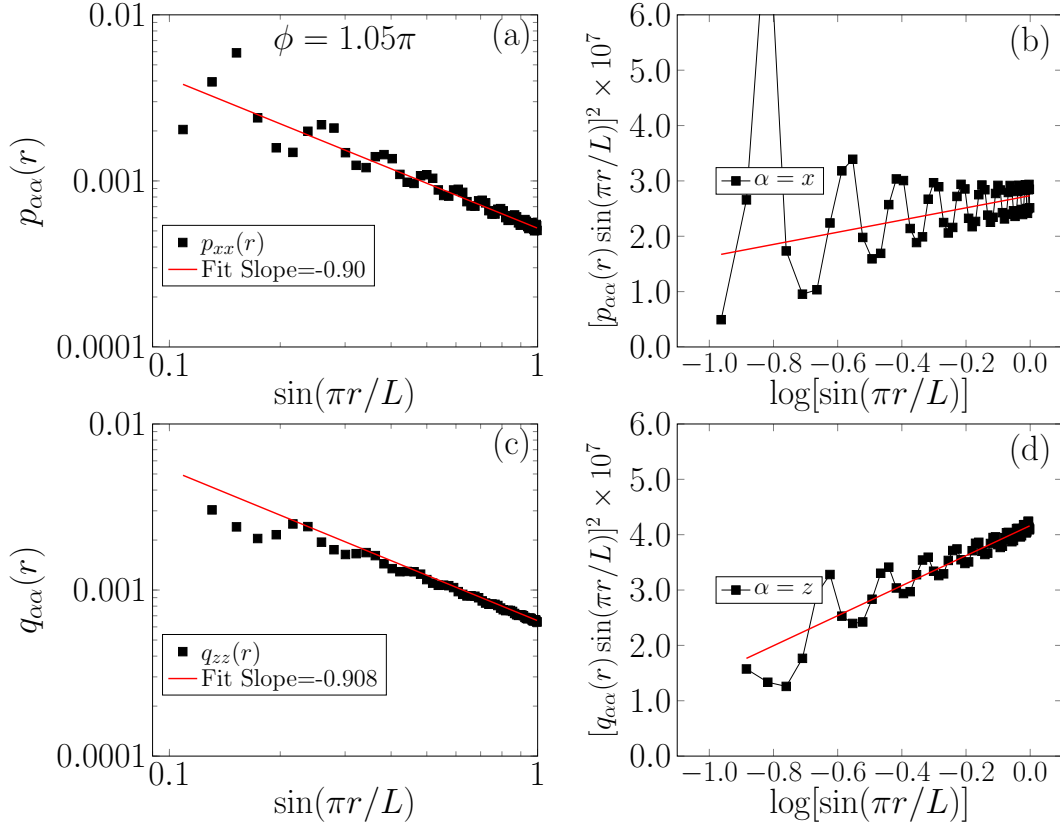


FIG. 14: (a)  $p_{xx}(r)$  and (c)  $q_{zz}(r)$  vs.  $\sin(\pi r/L)$  on a log-log scale; (b)  $(p_{xx}(r) \sin(\pi r/L))^2$  and (d)  $(q_{zz}(r) \sin(\pi r/L))^2$  plotted against  $\ln(\sin(\pi r/L))$ . DMRG numerics are carried out on a system of  $L = 144$  sites with periodic boundary conditions at  $\phi = 1.05\pi$ .  $p_{\alpha\alpha}(r)$  and  $q_{\alpha\alpha}(r)$  are then extracted from  $\langle S_1^\alpha S_{1+r}^\alpha \rangle$  using the nine-point formula.

In this section, we study the momentum  $\pm\pi/3$  oscillating components of the spin-spin correlation functions. An angle  $\phi = 1.05\pi$  is chosen as a representative example. The correlation functions  $\langle S_1^\alpha S_{1+r}^\alpha \rangle$  are calculated from DMRG numerics on a system of  $L = 144$  sites with a periodic boundary condition. As throughout the manuscript, to reach numerical convergence, up to  $m = 1000$  DMRG states were kept and tens of finite size sweeps were performed with a final truncation error of  $10^{-6}$ . We will neglect the uniform and momentum  $\pm 2\pi/3$  oscillating components of the correlation functions, since they decay faster than the staggered and momentum  $\pm\pi/3$  oscillating components at long distances. We denote the staggered component as  $s_{\alpha\alpha}(r)$  and the two momentum  $\pm\pi/3$  oscillating components as  $p_{\alpha\alpha}(r)$  and  $q_{\alpha\alpha}(r)$ . We expect that all of these nine correlation functions  $s_{\alpha\alpha}, p_{\alpha\alpha}, q_{\alpha\alpha}$  ( $\alpha = x, y, z$ ) behave as  $\sim \ln^{1/2}(\sin(\pi r/L))/\sin(\pi r/L)$  at long distances. Since  $s_{\alpha\alpha}$  has already been studied in the maintext, here we focus on  $p_{\alpha\alpha}$  and  $q_{\alpha\alpha}$ . A representative direction  $\alpha = x$  is chosen for  $p_{\alpha\alpha}$  and  $\alpha = z$  is chosen for  $q_{\alpha\alpha}$ .

In Fig. 14 (a) and (c),  $p_{xx}(r)$  and  $q_{zz}(r)$  are plotted against  $\sin(\pi r/L)$  on a log-log scale, both exhibiting a good linear relation with a slope  $\sim -0.9$  which is close to  $-1$  within 10% error. Due to the logarithmic correction, it is expected that the observed exponent is slightly smaller than the predicted value 1. To study the logarithmic factor, in Fig. 14 (b) and (d),  $(p_{xx}(r) \sin(\pi r/L))^2$  and  $(q_{zz}(r) \sin(\pi r/L))^2$  are plotted against  $\log(\sin(\pi r/L))$ . If the logarithmic factor is  $\ln^{1/2}(\sin(\pi r/L))$ , then a linear relation will be observed. We see from Fig. 14 (b) and (d) that the linearity is not good due to an oscillation with a six-site periodicity. In fact, such six-site oscillation is not unexpected. When applying the nine-point formula, the uniform component and the momentum  $\pm 2\pi/3$  components are neglected. These naturally introduce oscillations into the extracted values of  $s_{\alpha\alpha}, p_{\alpha\alpha}, q_{\alpha\alpha}$  with a six-site periodicity. On the other hand, since  $C_2/C_1$  is still close to 1 even very far away from the SU(2) symmetric point  $\phi = 5\pi/4$ ,  $s_{\alpha\alpha}$  dominates over  $p_{\alpha\alpha}, q_{\alpha\alpha}$ . The smallness of  $p_{\alpha\alpha}, q_{\alpha\alpha}$  means that they are more sensitive to the influence of the uniform and the momentum  $\pm 2\pi/3$  components. Indeed, Fig. 3 (d) in the maintext also contains oscillations, but much less prominent than those in Fig. 14 (b) and (d). We expect that the oscillations in Fig. 14 (b) and (d) can be reduced by going to larger system sizes.

### Finite size scaling of the exponents for the staggered parts of the correlation functions

In this section, we study the finite size scaling behaviors of the exponents for the staggered components  $s_{\alpha\alpha}(r)$  ( $\alpha = x, y, z$ ) of the spin-spin correlation functions  $\langle S_1^\alpha S_{r+1}^\alpha \rangle$  varying system size. The DMRG numerical results are shown in Fig. 15, where  $s_{\alpha\alpha}$  is extracted from the numerically calculated  $\langle S_1^\alpha S_{r+1}^\alpha \rangle$  using a three-point formula as explained in the main text. We show that by properly dividing  $s_{\alpha\alpha}$  by the factor of the logarithmic correction, the exponents are close to  $-1$  with remarkable precisions (error less than 0.2%) for all three system sizes  $L = 48, 72, 144$ . Thus the exponent nearly has no dependence on the system size at least when  $L$  is greater than 48.

In Fig. 15 (a, d, g),  $s_{\alpha\alpha}$  vs.  $\sin(\pi r/L)$  are plotted on a log-log scale for a system of  $L = 48, 72, 144$  sites, respectively. It can be seen that the slopes are already very close to  $-1$  (with an error within  $\sim 8\%$ ) for all three system sizes. The small deviations from  $-1$  is due to the logarithmic factor arising from the marginally irrelevant operator  $-\lambda \vec{J}_L \cdot \vec{J}_R$  as explained in the main text, where  $\lambda > 0$  is the coupling constant.

To get a better exponent, we will extract the logarithmic factor first, and then divide  $s_{\alpha\alpha}$  by the extracted logarithmic factor. In Fig. (b, e, h),  $[s_{\alpha\alpha}(r) \sin(\pi r/L)]^2$  vs.  $\log(\sin(\pi r/L))$  are plotted for a system of  $L = 48, 72, 144$  sites, respectively. The data can be fitted with a linear relation  $[s_{\alpha\alpha}(r) \sin(\pi r/L)]^2 = A_\alpha \log(\frac{L}{\pi} \sin(\frac{\pi r}{L})) + B_\alpha$ , and the good linear fits indicate logarithmic factors with a power of  $1/2$  consistent with Eq. (4) in the main text. Next define  $w_{\alpha\alpha}$  as

$$w_{\alpha\alpha}(r) = \frac{s_{\alpha\alpha}(r)}{\sqrt{A_\alpha \log(\frac{L}{\pi} \sin(\frac{\pi r}{L})) + B_\alpha}}, \quad (117)$$

so that the logarithmic factor is removed from  $s_{\alpha\alpha}$ . In Fig. 3 (c, f, i),  $w_{\alpha\alpha}(r)$  vs.  $\sin(\pi r/L)$  are plotted on a log-log scale for a system of  $L = 48, 72, 144$  sites, respectively, all exhibiting slopes close to  $-1$  with remarkable precisions (less than 0.2%). Therefore we see that essentially there is no finite size dependence of the exponent.

### Finite size scaling of $C_1/C_2$

In this section, we study the dependence of the ratio  $C_1/C_2$  on the system size for different angles  $\phi$ . Here we use a method independent from the one used in the main text. An open boundary condition is adopted here, and spin-spin correlations are evaluated between the sites at  $r_1 = L/4$  and  $r_2 = 3L/4$ . To reach numerical convergence,  $m = 800$  DMRG states are used and up to 10 finite size sweeps are performed with a final truncation error of  $10^{-9}$ .

Given the above setup,  $\langle S_{r_1}^\alpha S_{r_2}^\alpha \rangle$  are computed for different  $L$ . As shown in Fig. 16, when displayed in a log-log scale, a perfect linear behavior is observed as in the main text for the staggered part of the correlation functions. Similarly to Fig. 3 in the maintext,  $x$  and  $y$  correlations numerically coincide at large distances, while the  $z$  correlation appears as a parallel straight line with approximately the same slope but different intercept compared with the other two correlations.

By extrapolating the intercepts with the y-axis, the ratio  $C_1/C_2$  can be extracted. Fig. 16 (c) shows a very weak dependence of  $C_1/C_2$  on system sizes for all the values of  $\phi$  within the AFM phase of the model. We have verified that the results are consistent with those obtained using chains with periodic boundary conditions, and therefore provide further evidence that the numerical results do not depend on the choice of boundary conditions.

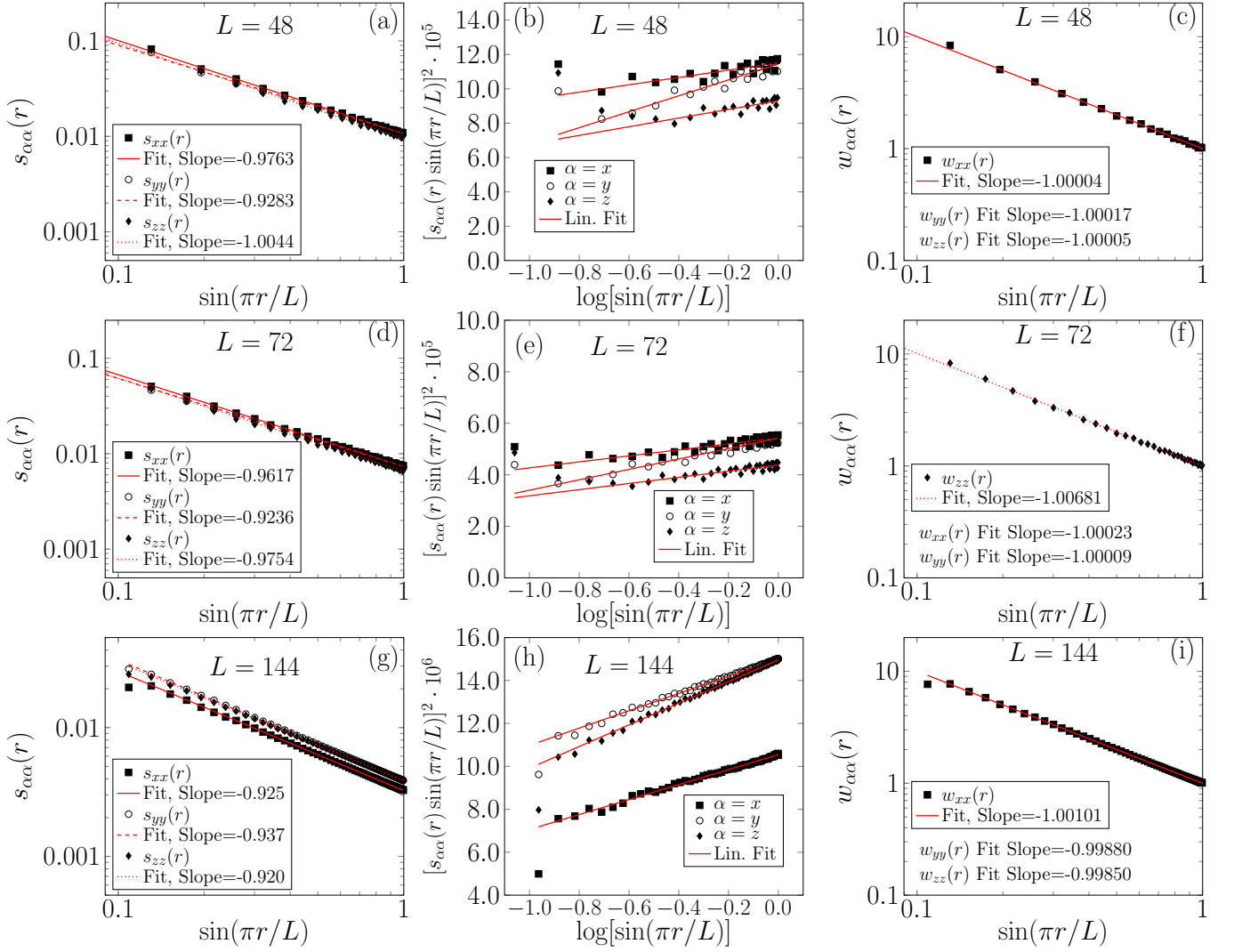


FIG. 15:  $s_{\alpha\alpha}(r)$  ( $\alpha = x, y, z$ ) vs.  $\sin(\pi r/L)$  on a log-log scale for a finite size system of (a) 48, (d) 72 and (g) 144 sites;  $[s_{\alpha\alpha}(r) \sin(\pi r/L)]^2$  vs.  $\log(\sin(\pi r/L))$  for a finite size system of (b) 48, (e) 72 and (h) 144 sites;  $w_{\alpha\alpha}(r)$  vs.  $\sin(\pi r/L)$  on a log-log scale for a finite size system of (c) 48, (f) 72 and (i) 144 sites, where  $w_{\alpha\alpha}(r)$  is defined as  $s_{\alpha\alpha}(r)$  divided by the logarithmic factor as explained in the text. In (a,b,d,e,g,h),  $s_{\alpha\alpha}(r)$  is the staggered part of the correlation function  $\langle S_1^\alpha S_{r+1}^\alpha \rangle$  extracted from a three-point formula as explained in the main text. In (c,f,i), all three curves of  $w_{\alpha\alpha}$  for  $\alpha = x, y, z$  collapse, hence the data of only one spin direction are shown for each system size. Periodic boundary conditions are used in DMRG numerical computations.

## THE FM PHASE

In this section, we discuss the ordered phase. Due to the equivalence established by  $\mathcal{T}_3$  as mentioned in the main text, we will use interchangeably the angles  $\phi$  and  $2\pi - \phi$  and do not distinguish between the two.

### Spin orientations with $O_h \rightarrow D_4$ symmetry breaking

We discuss the  $O_h \rightarrow D_4$  symmetry breaking. We show that the spin orientations

$$\langle \vec{S}_1 \rangle = S' \hat{z}, \langle \vec{S}_2 \rangle = S'' \hat{z}, \langle \vec{S}_3 \rangle = S'' \hat{z}, \quad (118)$$

are invariant under  $\langle R_a T_a R(\hat{z}, \pi) R_I I R(\hat{z}, \pi), T(R_a T_a)^{-1} R_I I R_a T_a \rangle \cong D_4$ , where  $D_4$  is the symmetry group of a square.

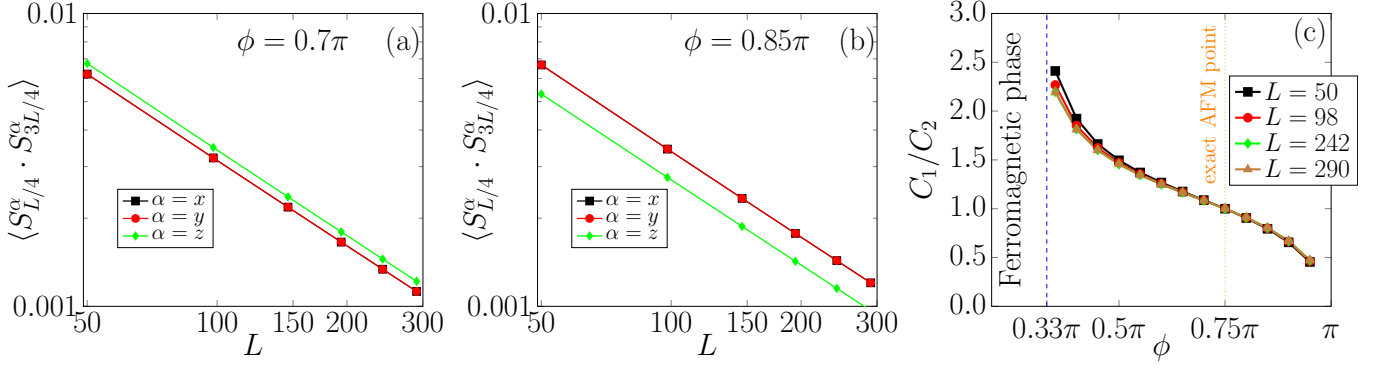


FIG. 16:  $\langle S_{L/4}^\alpha S_{3L/4}^\alpha \rangle$  ( $\alpha = x, y, z$ ) as functions of system size  $L$  in a log-log plot at (a)  $\phi = 0.7\pi$  and (b)  $\phi = 0.85\pi$ , and (c)  $C_1/C_2$  extracted from the spin-spin correlations as a function of  $\phi$  within the AFM phase.

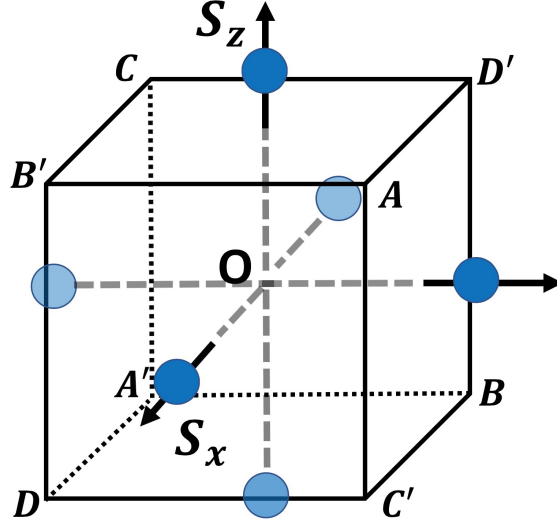


FIG. 17: "Center of mass" directions represented by the six blue solid circles for the  $O_h \rightarrow D_4$  symmetry breaking.

Consider a general spin configuration within a unit cell,

$$\vec{S}_1 = \begin{pmatrix} x_1 \\ y_1 \\ z_1 \end{pmatrix}, \vec{S}_2 = \begin{pmatrix} x_2 \\ y_2 \\ z_2 \end{pmatrix}, \vec{S}_3 = \begin{pmatrix} x_3 \\ y_3 \\ z_3 \end{pmatrix}. \quad (119)$$

Under  $R_a T_a \cdot R(\hat{z}, \pi) \cdot R_I I \cdot R(\hat{z}, \pi)$ , Eq. (119) is mapped to

$$\begin{aligned} R_a T_a \cdot R(\hat{z}, \pi) \cdot R_I I \cdot R(\hat{z}, \pi) : \vec{S}_1 &\rightarrow \begin{pmatrix} -x_1 \\ -y_1 \\ z_1 \end{pmatrix} \rightarrow \begin{pmatrix} z_3 \\ y_3 \\ -x_3 \end{pmatrix} \rightarrow \begin{pmatrix} z_3 \\ -y_3 \\ x_3 \end{pmatrix} \rightarrow \begin{pmatrix} y_1 \\ -x_1 \\ z_1 \end{pmatrix} \\ \vec{S}_2 &\rightarrow \begin{pmatrix} -x_2 \\ -y_2 \\ z_2 \end{pmatrix} \rightarrow \begin{pmatrix} z_2 \\ y_2 \\ -x_2 \end{pmatrix} \rightarrow \begin{pmatrix} z_2 \\ -y_2 \\ x_2 \end{pmatrix} \rightarrow \begin{pmatrix} y_3 \\ -x_3 \\ z_3 \end{pmatrix} \\ \vec{S}_3 &\rightarrow \begin{pmatrix} -x_3 \\ -y_3 \\ z_3 \end{pmatrix} \rightarrow \begin{pmatrix} z_1 \\ y_1 \\ -x_1 \end{pmatrix} \rightarrow \begin{pmatrix} z_1 \\ -y_1 \\ x_1 \end{pmatrix} \rightarrow \begin{pmatrix} y_2 \\ -x_2 \\ z_2 \end{pmatrix}, \end{aligned} \quad (120)$$

in which the arrows indicate subsequent applications of the operators in  $R_a T_a \cdot R(\hat{z}, \pi) \cdot R_I I \cdot R(\hat{z}, \pi)$  separated by

dot. Under  $T \cdot (R_a T_a)^{-1} \cdot R_I I \cdot R_a T_a$ , Eq. (119) is mapped to

$$\begin{aligned}
T \cdot (R_a T_a)^{-1} \cdot R_I I \cdot R_a T_a : \vec{S}_1 &\rightarrow \begin{pmatrix} z_2 \\ x_2 \\ y_2 \end{pmatrix} \rightarrow \begin{pmatrix} -x_2 \\ -z_2 \\ -y_2 \end{pmatrix} \rightarrow \begin{pmatrix} -y_1 \\ -x_1 \\ -z_1 \end{pmatrix} \rightarrow \begin{pmatrix} y_1 \\ x_1 \\ z_1 \end{pmatrix}, \\
\vec{S}_2 &\rightarrow \begin{pmatrix} z_3 \\ x_3 \\ y_3 \end{pmatrix} \rightarrow \begin{pmatrix} -x_1 \\ -z_1 \\ -y_1 \end{pmatrix} \rightarrow \begin{pmatrix} -y_3 \\ -x_3 \\ -z_3 \end{pmatrix} \rightarrow \begin{pmatrix} y_3 \\ x_3 \\ z_3 \end{pmatrix}, \\
\vec{S}_3 &\rightarrow \begin{pmatrix} z_1 \\ x_1 \\ y_1 \end{pmatrix} \rightarrow \begin{pmatrix} -x_3 \\ -z_3 \\ -y_3 \end{pmatrix} \rightarrow \begin{pmatrix} -y_2 \\ -x_2 \\ -z_2 \end{pmatrix} \rightarrow \begin{pmatrix} y_2 \\ x_2 \\ z_2 \end{pmatrix}.
\end{aligned} \tag{121}$$

Clearly, Eq. (118) is invariant under  $R_a T_a \cdot R(\hat{z}, \pi) \cdot R_I I \cdot R(\hat{z}, \pi)$  and  $T \cdot (R_a T_a)^{-1} \cdot R_I I \cdot R_a T_a$ . In addition, the invariant spin configurations under both operations can only be of the form given in Eq. (118).

Next we prove that  $\langle R_a T_a R(\hat{z}, \pi) R_I I R(\hat{z}, \pi), T(R_a T_a)^{-1} R_I I R_a T_a \rangle$  is isomorphic to  $D_4$ . The generator-relation representation of  $D_4$  is

$$D_4 = \langle a, b | a^4 = b^2 = (ab)^2 = e \rangle. \tag{122}$$

We make the following identification:  $a = R_a T_a \cdot R(\hat{z}, \pi) \cdot R_I I \cdot R(\hat{z}, \pi)$ , and  $b = T \cdot (R_a T_a)^{-1} \cdot R_I I \cdot R_a T_a$ . We show that  $a$  and  $b$  satisfy the relations in Eq. (122). Since the actions of  $a$  and  $b$  in the spin space are  $R(\hat{z}, \pi/2)$  and the reflection to the plane  $ACA'C'$  shown in Fig. 17, respectively, it is straightforward to verify that the relations in Eq. (122) are satisfied by restricting the actions to the spin space. Then it is enough to verify the relations for the spatial components. Firstly, for  $a^4$  we have

$$(T_a I)^4 = T_a (I T_a I) T_a (I T_a I) = T_a T_{-a} T_a T_{-a} = e. \tag{123}$$

Secondly, for  $b^2$ , we have

$$(T_a^{-1} I T_a)^2 = T_{-a} I (T_a T_{-a}) I T_a = T_{-a} I^2 T_a = T_{-a} T_a = e. \tag{124}$$

Thirdly, for  $(ab)^2$ , we have

$$(T_a I T_a^{-1} I T_a)^2 = T_{3a}^2, \tag{125}$$

which is  $e$  modulo  $T_{3a}$ . This shows that  $\langle R_a T_a R(\hat{z}, \pi) R_I I R(\hat{z}, \pi), T(R_a T_a)^{-1} R_I I R_a T_a \rangle$  is isomorphic to a subgroup of  $D_4$ . On the other hand, by only considering the actions within the spin space, one can show that there are at least eight elements within the group  $\langle R_a T_a R(\hat{z}, \pi) R_I I R(\hat{z}, \pi), T(R_a T_a)^{-1} R_I I R_a T_a \rangle$ . Thus we conclude that it is isomorphic to  $D_4$ .

### ED results on the ground state degeneracies

The model is equivalent to a ferromagnetic Heisenberg model at  $\phi = 0.25\pi$ . We have verified numerically that the ferromagnetic phase extends in the region  $0.12\pi \lesssim \phi < \phi_c \approx 0.33\pi$ . Therefore, without loss of generality, in this section we investigate the low energy properties of the model for  $\phi = 0.2\pi$ .

ED on spin  $S = 1/2$  chain with periodic boundary conditions finds a degenerate ground state subspace with dimension 6 at zero field as shown by the blue box under the  $h = 0$  column in Table III. This subspace is separated from the excited states by a relatively small gap  $\sim 10^{-3}$  for a chain with length  $L = 21$  sites. These results are compatible with a symmetry breaking pattern from  $O_h$  to  $D_4$ . The 6-fold degeneracy of  $O_h \rightarrow D_4$  symmetry breaking is equivalent to the number of faces of a cube shown in Fig. 17, with normal directions pointing along the cartesian axes directions  $\hat{\alpha} = \pm\hat{x}, \pm\hat{y}, \pm\hat{z}$ .

To further test the symmetry breaking patterns, we apply a small uniform magnetic field in such a way that the low lying sextet do not hybridize with excited states above the gap in the spectrum. In particular, we have applied a magnetic field of strength  $h_{\hat{y}} = 5 \times 10^{-6}$  along the  $y$ -direction such that the constraint  $10^{-6} \ll h_{\hat{y}} L \simeq 10^{-4} \ll 10^{-3}$  is fulfilled. The column of  $h_{\hat{y}}$  in Table III shows that there is a unique ground state separated by a gap  $E_2 - E_1 \simeq 5 \times 10^{-5}$

	$h=0$	$h_{\hat{y}} = 5 \times 10^{-6}$	$h_{\hat{n}_a} = 5 \times 10^{-6}$	$h_{\hat{n}_I} = 5 \times 10^{-6}$
1	-3.54113	-3.54118	-3.54118	-3.54118
2	-3.54113	-3.54113	-3.54118	-3.54118
3	-3.54113	-3.54113	-3.54118	-3.54113
4	-3.54113	-3.54113	-3.54108	-3.54113
5	-3.54113	-3.54113	-3.54108	-3.54108
6	-3.54113	-3.54108	-3.54108	-3.54108
7	-3.53799	-3.53801	-3.53802	-3.53802
8	-3.53799	-3.53798	-3.53799	-3.53798

TABLE III: Energies of several lowest lying states computed with Lanczos Exact Diagonalization. Numerics are performed on a system containing  $L = 21$  sites with a periodic boundary condition.

from a quartet of excited states. Above the first six states, there is a gap  $E_7 - E_6 \simeq 10^{-3}$  as without field, showing that the field is just acting within the low energy sextet.

We also apply a small magnetic field along the direction of one of the eight corners of the cube,  $h_{\hat{n}} = \frac{1}{\sqrt{3}}(1, 1, 1)$ . As shown in the column  $h_{\hat{n}_a}$  in Table III, the 6-fold degenerate manifold splits into two triplet of states: Three states pointing to the directions  $+\hat{x}, +\hat{y}, +\hat{z}$  and the other three to opposite direction  $-\hat{x}, -\hat{y}, -\hat{z}$ . This is again consistent with the symmetry breaking pattern shown in Fig. 17.

We finally apply a small magnetic field point to the middle point of one of the twelve edges of the cube,  $h_{\hat{n}_I} = \frac{1}{\sqrt{2}}(1, 0, -1)$ . As shown in the column  $h_{\hat{n}_I}$  in Table III, the 6-fold degenerate manifold splits into three doublets of states: Two states pointing to the directions  $+\hat{x}, -\hat{z}$ , two states pointing to  $+\hat{y}, -\hat{y}$ , and two states pointing to  $-\hat{x}, \hat{z}$ . This is again consistent with the symmetry breaking pattern shown in Fig. 17.

### DMRG results on the correlation functions in the FM phase

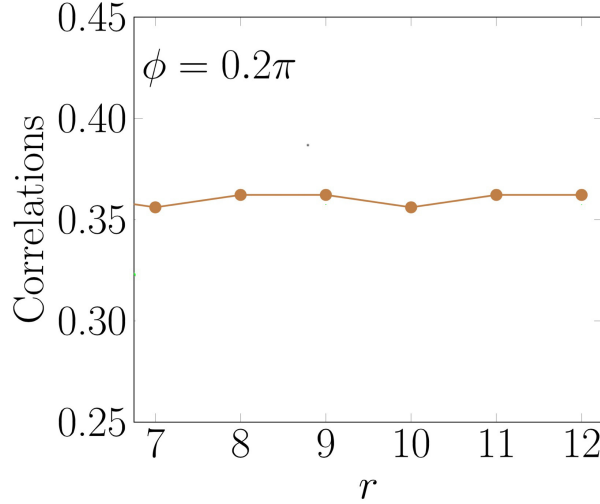


FIG. 18:  $\langle S_1^z S_{r+1}^z \rangle$  at  $h_z = 10^{-4}$  along  $\hat{z}$ . All other correlation functions vanish including  $\langle S_1^\alpha S_{r+1}^\alpha \rangle$  ( $\alpha = x, y$ ) and all cross correlations. Hence, they are not displayed.

We have numerically computed the correlation functions under different fields using DMRG numerics on a system with  $L = 24$  sites with a periodic boundary condition. Fig. 18 shows  $\langle S_1^z S_{r+1}^z \rangle$  with  $h_z = 10^{-4}$  along  $\hat{z}$ , and the pattern is consistent with Eq. (118). All other correlation functions vanish, including  $\langle S_1^x S_{r+1}^x \rangle$ ,  $\langle S_1^y S_{r+1}^y \rangle$ , and all cross correlations  $\langle S_1^\alpha S_{r+1}^\beta \rangle$  ( $\alpha \neq \beta$ ). The results are again consistent with the  $O_h \rightarrow D_4$  symmetry breaking.

- 
- [1] M. S. Dresselhaus, G. Dresselhaus, and A. Jorio, *Applications of Group Theory to the Physics of Solids* (Springer, New York, 2008) 1st ed.
- [2] P. Calabrese and J. Cardy, *J. Phys. A* **42**, 504005 (2009).
- [3] H. S. M. Coxeter, and W. O. Moser, *Generators and their relations for discrete groups* (Berlin: Springer 1965).
- [4] S. Eggert and I. Affleck, *Phys. Rev. B* **46**, 10 866 (1992).
- [5] I. Affleck, D. Gepner, H. J. Schulz, and T. Ziman, *J. Phys. A: Math. Gen.* **22**, 511 (1989).
- [6] J. Cardy, *Scaling and Renormalization in Statistical Physics* (Cambridge University Press, Cambridge, 1996).
- [7] Let  $V_1$  and  $V_2$  be two  $\mathbb{R}$ -linear irreducible representations of the group  $F$ . Let  $\phi : V_1 \times V_2 \rightarrow \mathbb{R}$  be a bilinear form satisfying  $\phi(fv_1, v_2) = \phi(v_1, f^{-1}v_2)$  for any  $v_1 \in V_1, v_2 \in V_2, f \in F$ . Then  $\phi$  induces a map  $\phi^* : V_1 \rightarrow V_2^*$ , in which  $V_2^*$  is the dual space of  $V_2$ , *i.e.*,  $V_2^*$  consists of all  $\mathbb{R}$ -linear functions on  $V_2$ . Note that  $V_2^*$  is naturally a representation of  $F$ . The property of  $\phi$  ensures that  $\phi^*$  commutes with  $F$ . Then by Schur's lemma,  $\phi^*$  is either 0 or an isomorphism. Thus if  $V_1$  and  $V_2^*$  are two different irreducible representations,  $\phi^*$  has to be zero, hence  $\phi = 0$ . Since  $\mathbb{C}$ -linear spaces are also  $\mathbb{R}$ -linear and the inner product on a complex Hilbert space is bilinear in  $\mathbb{R}$  by restricting the coefficients in  $\mathbb{C}$  to  $\mathbb{R}$ , the above conclusion holds also for complex irreducible representations.
-